Behaviour and design of square cold-formed concrete-filled double-skin stiffened slender columns

M.F. Hassanein [a,b], Song-qi Jiang [a], Yong-Bo Shao [a,*], K.A. Cashell [c]

[a] School of Architecture and Civil Engineering, Xihua University, Chengdu 610039, PR China
[b] Department of Structural Engineering, Faculty of Engineering, Tanta University, Tanta, Egypt
[c] Department of Civil Environmental and Geomatic Engineering, UCL, London, UK

ARTICLE INFO

ABSTRACT

Concrete-filled double-skin stiffened steel tubular (CFD-SSST) slender columns with a square inner tube, a cold-formed stiffened outer tube, and concrete infill between the two steel sections are examined in this paper. To the best of the authors' knowledge, while the behaviour of short columns has been investigated, the behaviour of these kinds of slender columns has not. As a result, a finite element model has been development and its details are provided, along with a validation against test data that is currently available. An extensive parametric study is conducted using the model to investigate the behaviour of CFD-SSST slender columns with varying geometric and material properties. A technique for defining intermediate-length and long columns is suggested based on an examination of the strain distributions in the cross-section. It is demonstrated that the slenderness ratio, which influences both the failure mode and the capacity, is a crucial parameter in the behaviour of CFD-SSST columns. The yield strength of the outer steel tube, the strength of the sandwiched concrete, and the width-to-thickness ratio of the outer tube are all found to be significant factors for intermediate-length columns, but only the former is found to have a significant impact on long columns. Because there is currently a lack of specific guidance, the final strengths are compared with several design approaches that were appropriately modified to account for different components forming the cross-section of CFD-SSST slender columns. The design model by AS/NZS 2327 standard (2017) was found to provide well the strengths of CFD-SSST slender columns, and therefore recommended for design.

1. Introduction

Innovative composite columns known as concrete-filled double-skin tubular (CFD-ST) columns have been proposed recently, especially for structural applications involving high loads. An outer steel tube, an inner steel tube positioned concentrically, and concrete infilled between the two steel sections make up these CFD-ST columns. An example that is used in electrical grid networks in China is illustrated in Fig. 1(a). As a result, they resemble conventional concrete-filled steel tubular (CFST) members, except that they lack core concrete and have an inner steel tube. Many of the benefits of CFST members are also present in CFD-ST columns, but they perform better in a number of areas, such as load capacity, durability, flexural rigidity, fire resistance, constructability, energy absorption, and dissipation capacity [1–7].

As illustrated in Fig. 1(b), the conventional fabrication technique for the outer tube of square CFST columns involves welding four plates at the corners; the Ruifeng International Commercial Building in Hanzhou, for instance, used these components [7]. Even though these built-up sections have a reasonable load-capacity, prior studies have shown that they may undergo local buckling before reaching their full capacity, and the outer steel tube may crack as a result of welding defects [8,9]. In order to enhance the resistance of conventional CFST columns, stiffeners were welded and added to the outer steel section to come up with concrete-filled stiffened steel tubular (CFSST) columns, as shown in Fig. 1(c) [10–12]. However, using these stiffeners increases the fabrication cost of the members based on the large numbers of weld lines, as used in Taibei 101 Building. Accordingly, stiffened sections made by welding four lipped angle sections together have been suggested, to reduce largely the number of weld lines, as presented in Fig. 1(d) [13]. Recently, large warehouses and commercial buildings in South Korea

---

* Corresponding author.

E-mail addresses: mostafa.fahmi@f-eng.tanta.edu.eg (M.F. Hassanein), songqi_jiang@163.com (S.-q. Jiang), shaoyb@mail.xhu.edu.cn (Y.-B. Shao), k.cashell@ucl.uk (K.A. Cashell).

have made extensive use of this cross-section [13].

Zhang and Chen [14] investigated the axial behaviour of CFSST short columns and discovered that shear dominates the failure modes. Additionally, it was demonstrated that the stiffeners had a strong bond with the concrete until the specimens started to fail, and that their presence had a noticeable positive impact on the CFSST columns' ultimate resistance. CFSST short columns with stainless steel tubes were the subject of an experimental investigation by Dabaon et al. [15], which was supported by numerical analysis [16]. It was demonstrated that the columns' failure in various cross-sections was caused by local buckling of the outer steel tube, preventing a complete loss of bearing capacity at that cross-section. Generally speaking, CFSST columns made from cold-formed plates with four lipped angles welded together perform better than conventional CFSST columns. Given the outstanding performance of CFSST columns, a concrete-filled double-skin stiffened steel tubular (CFD-SSST) column was proposed as a further development to enhance their performance by removing core concrete and adding an internal steel cross-section (Fig. 2).

Extensive research has been conducted to study the behaviour of CFD-SSST columns in recent years [e.g. 17–24]. Wang et al. [17] conducted an experimental study on the axial behaviour of CFDSST short columns, which are concrete-filled stiffened dual steel tubular columns. The test results indicated that the inner circular CFST component can be used to effectively improve the ultimate resistance and ductility of CFD-SSST columns. Zhang et al. [18] performed a numerical study on the axial behaviour of CFDSST short columns filled with ultra-high strength concrete (UHSC) and found that the strength of the sandwiched concrete is highly influential on the ultimate resistance of CFDSST columns. Similarly, Wang et al. [19] experimentally studied the axial behaviour of CFDSST slender columns, and showed that they offer similar ultimate strength and ductility compared with CFSST columns, but with a smaller weight. Wang et al. [21,22] conducted studies on the behaviour of CFD-SSST columns under eccentric axial loading and Wang et al. [23,24] investigated the seismic behaviour of both CFSST and CFD-SSST sections, showing that both cross-sections have stable hysteretic loops.

Circular cross-sections in composite columns typically exhibit superior performance compared to square ones due to better concrete confinement, higher load capacity, and a more uniform stress distribution. However, square cross-sections offer advantages in constructability and cost-effectiveness. Building on the authors' recent experimental investigation of short CFD-SSST columns [25], this study focuses on the
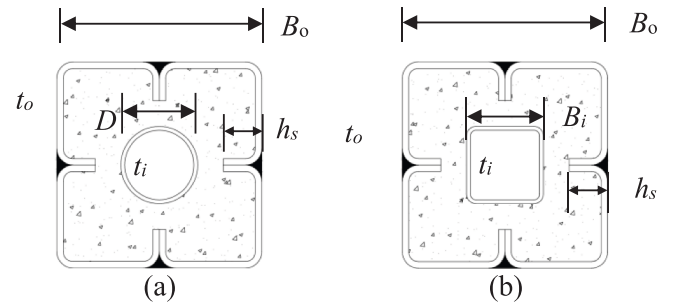

Fig. 2. Cross-sections of CFD-SSST columns with (a) circular and (b) square inner steel sections.

behaviour of slender CFD-SSST columns with square outer and inner steel tubes, as illustrated in Fig. 2(b). In practice, columns are usually slender and prone to overall buckling, making this an important area of study. While overall buckling in conventional CFST slender columns has been investigated since the 1960s [26,27], CFD-SSST slender columns remain largely unexplored.

Recent studies have advanced understanding of slender composite columns. Schurgacz et al. [28] conducted experimental tests on composite columns in one- and two-storey configurations using high-performance materials—steel with yield strengths up to 1000 MPa and concrete up to 100 MPa—demonstrating that while material strength significantly enhances the load-bearing capacity of short columns, its effect diminishes with increasing slenderness. Zhao et al. [29] examined the behaviour of slender CFDST columns and beams using stainless steel outer tubes, exploring parameters such as material strength, hollow ratio, and eccentricity. Their results were evaluated against several design codes, including those by Han et al. [30], GB 50936–2014 [31], and AISC 360–16 [32], with Han et al.'s method yielding the most accurate predictions. Hassanein et al. [33] numerically studied slender CFDSST columns featuring cold-formed, stiffened outer tubes, and found the AS/NZS 2327 standard [34] provided the most reliable design predictions. Similarly, Zhang et al. [20] investigated slender, square ultra-high strength CFDSST columns with a concentrically positioned circular inner steel tube. They identified concrete strength, outer tube yield strength, and the width-to-thickness ratio as key parameters influencing the axial capacity of intermediate-length columns, with concrete strength having the greatest impact on long
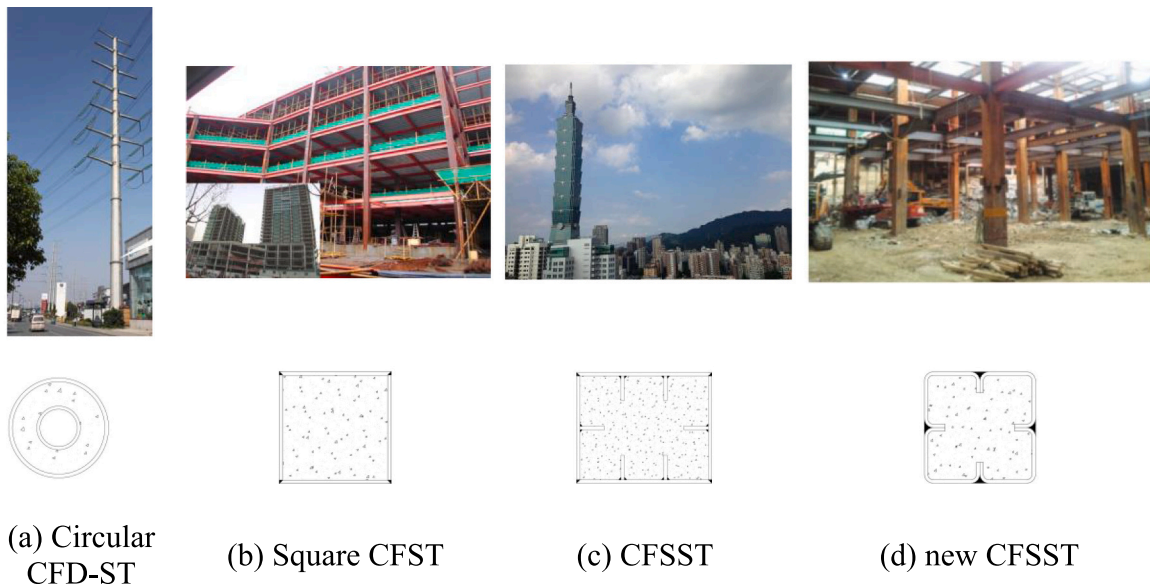

(a) Circular CFD-ST   (b) Square CFST   (c) CFSST   (d) new CFSST

Fig. 1. Typical examples of concrete-filled columns.

columns. They recommended the AISC 360–16 [32] method, with appropriate modifications, for design of these novel sections.

Therefore, the primary objective is to provide the scientific community and researchers information about the strength and behaviour characteristics of CFD-SSST columns of various lengths (i.e., under different failure modes). Overall, by expanding the pool of results available, this could result in a wider use of these columns in practice. To examine the behaviour and strength of CFD-SSST slender columns, a finite element (FE) model has been established and validated using the test results that are currently available. In order to investigate the effects of different design parameters on the global buckling behaviour, capacity, and failure mode, a comprehensive parametric analysis was conducted. A design method was proposed and presented to predict the compressive capacity of these slender members based on the findings of this paper.

2. Development of the FE model

Currently, no experimental data are available for concrete-filled double-skin stiffened steel tubular (CFD-SSST) slender columns. Therefore, to establish a robust foundation for investigating their behaviour, finite element (FE) models were first developed to simulate the response of CFD-SSST short columns and conventional concrete-filled steel tubular (CFST) slender columns. These preliminary simulations enabled the calibration and validation of the modelling approach. The FE model was validated against multiple sets of experimental data available in the literature [11,19,25,35,36] to ensure it could accurately predict both the global behaviour and the ultimate strength of composite columns. The numerical analyses were conducted using the commercial finite element software ABAQUS [37]. For slender columns, the accuracy of the simulation is particularly sensitive to boundary conditions and initial geometric imperfections, both of which significantly influence overall buckling and ultimate capacity. These aspects are addressed in detail in subsequent sections.

2.1. Material models

The CFD-SSST columns consist of concrete filled between two concentrically-located square hollow steel tubes where the outer steel tube is made with four lipped angles of cold-formed plates and lips which can be regarded as longitudinal stiffeners. Gardner and Yun [38] found that a rounded stress-strain curve accurately captures the behaviour of cold-formed steel elements without coatings. This finding has been further substantiated by Abdelrahman et al. [39]. However, it was found that considering strain hardening has limited effect on behaviour of the columns. For example, Tao et al. [40] and Wang et al. [17] showed that insignificant influence is provided by the development of strain hardening for square CFST short columns and concrete-filled double-tube stub columns with stiffeners, respectively. Accordingly, for the square outer and inner tubular sections of the existing composite columns, a material model for steel, which assumes elastic-perfectly plastic behaviour, is adopted. According to experimental date of steel material, the yield strength and modulus of elasticity is utilised.

As for concrete filled in sandwich area between outer lipped angles steel and inner square steel tube, it is under a triaxial stress condition when under a compressive load, because of the confinement provided from outer and inner steel tube. Due to the influence of confinement, the ultimate strength and ductility of concrete under compressive load are obviously improved. In this paper, the inelastic behaviour of concrete use the concrete damage plasticity (CDP) in the model. Fig. 3 shows the compressive behaviour of the confined concrete. According to Tao et al. [40], the curve is divided into three sections, which are showed as Eq. 1, Eq. 3 and Eq. 6.

$$\frac{\sigma}{f_c^{'}} = \frac{AX + BX^2}{1 + (A-2)X + (B+1)X^2} \quad (0 < \varepsilon < \varepsilon_{co}) \tag{1}$$
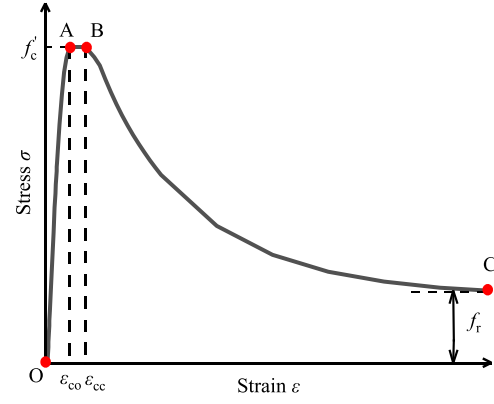

Fig. 3. Confined stress-strain (σ- ε) responses of concrete.

In the Eq. 1, σ is the stress. $f_c^{'}$ is the cylinder compressive strength of concrete. A=$\frac{E_c \varepsilon_{co}}{f_c^{'}}$ and B=$\frac{(A-1)^2}{0.55} - 1$. The value X is defined as $\frac{\varepsilon}{\varepsilon_{co}}$. The strain corresponding to the peak stress (ε_{co}) uses Eq. 2 to obtain.

$$\varepsilon_{c0} = 0.00076 + \sqrt{(0.626f_c^{'} - 4.33) \times 10^{-7}} \tag{2}$$

While stress is between ε_{co} and ε_{cc}, the section of the curve is a horizontal line, given as:

$$\sigma = f_c^{'} \quad (\varepsilon_{co} < \varepsilon < \varepsilon_{cc}). \tag{3}$$

$$\varepsilon_{cc} = \varepsilon_{c0} e^k \ , \ \text{and} \quad k = \left(2.9224 - 0.00367 f_c^{'}\right) \left(\frac{f_B}{f_c^{'}}\right)^{0.3124 + 0.002 f_c^{'}} \tag{4}$$

The confining stress f_B is defined as the following expression:

$$f_B = \frac{0.25 \cdot \left(1 + 0.027 f_y\right) \cdot e^{-0.02\sqrt{B^2 + D^2}}}{1 + 1.6 e^{-10} \cdot (f_c^{'})^{4.8}} \tag{5}$$

f_y is the yield stress of outer steel. B and D is the length and width of a steel tube of rectangular

cross-section. In this paper, the cross-section is square, so B is equal to D which is taken as square side length.

Finally, for $\varepsilon > \varepsilon_{cc}$, that is the descent stage, the curve is defined as Eq. 6.

$$\sigma = f_r + (f_c^{'} - f_r)\exp\left[-\left(\frac{\varepsilon - \varepsilon_{cc}}{\alpha}\right)^{\beta}\right](\varepsilon > \varepsilon_{cc}) \tag{6}$$

In this expression, $f_r = 0.1 f_c^{'}$, β is taken as 0.9 and $\alpha = 0.005 + 0.0075 \xi_c$ where ξ_c is the confinement factor of composite columns which is used to represent the confinement effect and is expressed by Eq. 7:

$$\xi_c = \frac{A_s f_y}{A_c f_c^{'}} \tag{7}$$

where A_s is the area of steel pipe and A_c is the area of sandwich concrete. In concrete material, the elastic modulus can be calculated as $4700\sqrt{f_c^{'}}$.

According to Mander et al. [41], the confined concrete strength can be replaced with f_{cc}, which is calculated by Eq. 8:

$$f_{cc} = f_c^{'} \left(-1.254 + 2.254\sqrt{1 + \frac{7.94 f_l^{'}}{f_c^{'}}}\right) \tag{8}$$

where $f_l^{'}$ is the effective confining stress, and is defined as the following expressions:

$$f_l^{'} = k_e f_l \tag{9}$$

$$f_l = \frac{2\sigma_{oh}t_o + \sigma_{sh}2t_o}{B - 2t_o} \qquad (10)$$

In these expressions, f_r is the confining stress, σ_{oh} is the horizontal stress of the outer steel tube and σ_{sh} is the horizontal stress of the stiffener. Moreover, σ_{oh} and σ_{sh} were considered as $0.19f_{yo}$ and $0.19f_{ys}$ as proposed by Sakino et al. [42] and Zhou et al. [43]. k_e is the confinement effectiveness coefficient which can be taken as 2/3 according to Huang et al. [44]. Thereinafter, there will be a comparison between the compressive strengthen $f_c^{'}$ and f_{cc}.

2.2. Modelling details

The finite element model comprises four lipped angle steel stiffeners, an inner steel tube, concrete infill, and two end plates. In the case of short columns, a local buckling mode known as "elephant foot buckling" was frequently observed near the column base. To mitigate this effect in the FE model, a clamping device was introduced, as illustrated in Fig. 7. For slender columns, however, the primary failure mode is global buckling; therefore, no clamping device was included in their corresponding FE models. A mesh sensitivity study was conducted using four mesh sizes: $B/5$, $B/10$, $B/15$, and $B/20$, where B is the side length of the cross-section. As shown in Fig. 4, the variation in mesh size had a minimal effect on the structural response. Consequently, a mesh size of $B/10$ was adopted for all analyses. To ensure numerical convergence, a finer mesh was used for the concrete compared to the steel tubes.

The concrete was modelled using eight-node brick elements with reduced integration (C3D8R), while the inner and outer steel tubes were modelled using four-node shell elements with reduced integration (S4R). The end plates were defined as rigid bodies, consistent with the use of high-strength steel in their fabrication. The interaction between steel and concrete was defined using surface-based contact with two components: tangential and normal behaviour. A friction coefficient of 0.6 was specified for the tangential interaction. For normal contact, "hard" contact was used to prevent penetration between the concrete and steel elements. The same contact definition was applied to the interfaces between the concrete and end plates, and between the steel and the clamping device. It should be noted that a friction coefficient of 0.6—or higher, if necessary—was used to avoid excessive rigid body displacement, which can cause convergence issues during the numerical analysis.

Different boundary conditions were adopted for the short and slender column models to reflect their distinct failure modes. For short columns, the base was fully fixed in all translational and rotational degrees of freedom, while the top was restrained in all directions except the axial direction (U_Z), allowing vertical displacement under loading. In contrast, slender columns were modelled with boundary conditions that allow for overall buckling. Specifically, the base was fixed in all directions except rotation about the x-axis (U_{RX}), while the top was restrained in all directions except axial translation (U_Z) and rotation about the x-axis (U_{RX}). This release of rotation in the x-direction was necessary to realistically capture the global buckling behaviour observed in slender members. A concentrated axial load was applied at the top of the model to initiate the response.

2.3. Residual stresses and initial imperfections

Previous studies have shown that residual stresses have a limited influence on the behaviour of composite structural elements such as concrete-filled steel tubes [20,46,47]. Specifically, Tao et al. [48] demonstrated that residual stresses have only a marginal effect on the performance of CFST short columns. According to the Chinese technical code for cold-formed thin-walled steel structures (GB 50018–2002 [49]), the strength enhancement due to the cold-forming process is not considered in welded structural sections, as welding can release some of the stresses introduced during cold-forming. Therefore, it is generally accepted that residual stresses from cold-forming and welding may partially offset each other [44]. Nevertheless, to evaluate the potential impact of residual stresses on the behaviour of the columns studied herein, a numerical analysis was conducted using the residual stress distribution proposed by Li et al. [50]. As illustrated in Fig. 5, the results with and without the inclusion of residual stresses differ by only 1.0 %, confirming their negligible influence. Consequently, residual stresses are not explicitly considered in the current study.

In contrast, initial geometric imperfections are known to have a more significant effect on the behaviour of slender composite columns than on short ones [48,51], and are therefore included in the finite element models. A convergence study was conducted to determine a suitable global imperfection amplitude. Three imperfection magnitudes were investigated: $L_e/500$, $L_e/1000$, and $L_e/5000$, where L_e is the effective length of the slender column. Based on the results shown in Fig. 6, an imperfection amplitude of $L_e/1000$ was selected for all slender column simulations [52].
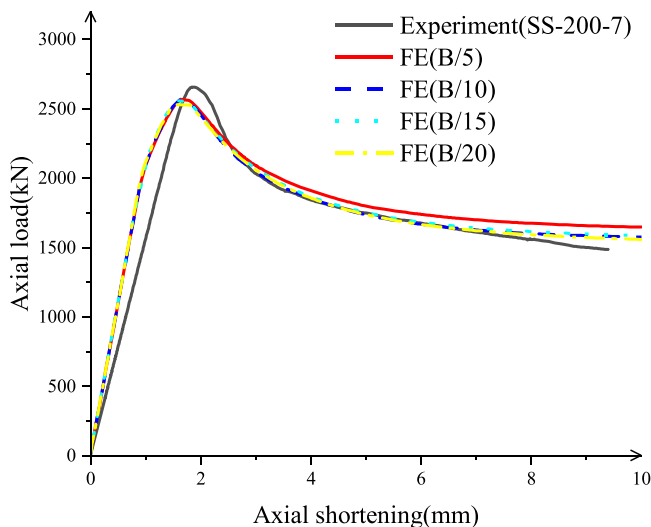

Fig. 4. Axial load *versus* axial shortening based on the mesh sensitivity analysis for column SS-200–7 [45].
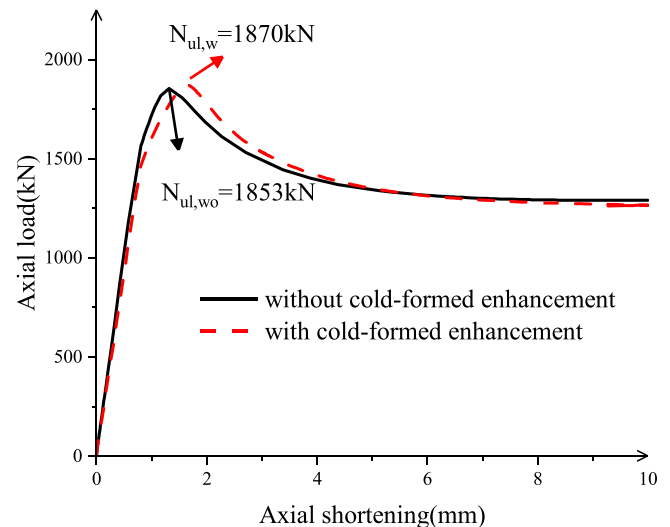

Fig. 5. Load *versus* axial shortening relationships for CFD-SSST column (SS-160–5) with and without enhance by cold-forming [45].
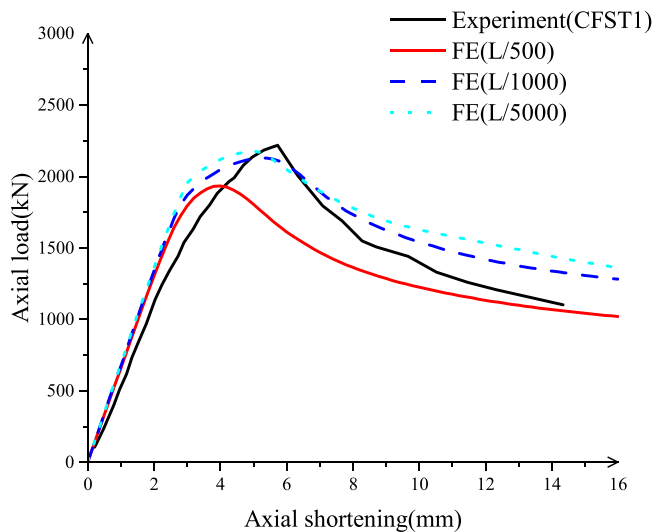
Fig. 6. Axial load *versus* axial shortening based on the initial imperfection sensitivity analysis for column CFST1 [53].

2.4. Validation of the numerical model

To ensure that the developed finite element (FE) model accurately captures all key behavioural characteristics, a comprehensive validation study was undertaken using reliable experimental data from comparable composite column types. Although no test data are currently available for CFD-SSST slender columns, the model was validated using results from square CFD-SSST short columns and various CFST columns reported in the literature. Specifically, the experimental data were sourced from Zhang et al. [45], Huang et al. [54], and Zhang et al. [53].

Table 1 presents the geometric details and ultimate strengths obtained from both the experimental results and the FE simulations, denoted as $N_{ul,Exp}$ and $N_{ul,FE}$, respectively. In this table, B_o and t_o refer to the side length and thickness of the outer steel tube, while B_i and t_i refer to the side length and thickness of the inner steel tube. All columns considered were square in cross-section, except for specimen CFST1 [53], which was rectangular with a cross-section of 300 mm (depth) × 100 mm (width), as indicated in Table 1. The height of all short columns (L_o) was taken as three times the side length of the outer tube (B_o). Fig. 7

The yield strengths of the outer and inner steel tubes are denoted by f_{yo} and f_{yi}, respectively. The compressive strength of the concrete was initially measured as the cube strength (f_{cu}), and then converted into the cylindrical compressive strength f_c'. The FE simulations were conducted using both f_c' and the confined concrete strength f_{cc} to obtain $N_{ul,FE}$ values and the full axial response of the columns. As shown in Table 1, the model using f_c' more accurately captures the ultimate capacity, with a mean $N_{ul,FE}/N_{ul,Exp}$ ratio of 0.96 and a coefficient of variation (COV) of 0.068. By contrast, using f_{cc} results in a mean ratio of 1.10 and a higher COV of 0.083, indicating greater variability. Furthermore, Figs. 8 and 9 illustrate the axial load–deflection responses and the axial load versus axial strain curves for both the outer steel tube (OST) and inner steel tube (IST), comparing numerical and experimental results. The FE model is shown to reliably replicate the key behavioural features of the specimens, including ultimate strength, initial stiffness, and post-peak softening. While the model slightly overestimates stiffness compared to experimental observations, its overall predictive performance is satisfactory for the intended analyses.

For slender columns, global (overall) buckling is expected to be the dominant failure mode, whereas local buckling tends to occur in short columns. As illustrated in Fig. 10, the FE model effectively captures both local buckling in short columns and global buckling in slender columns, in line with observed structural behaviour. In summary, the comparison

Table 1
Details and strengths of the columns used in the validation.

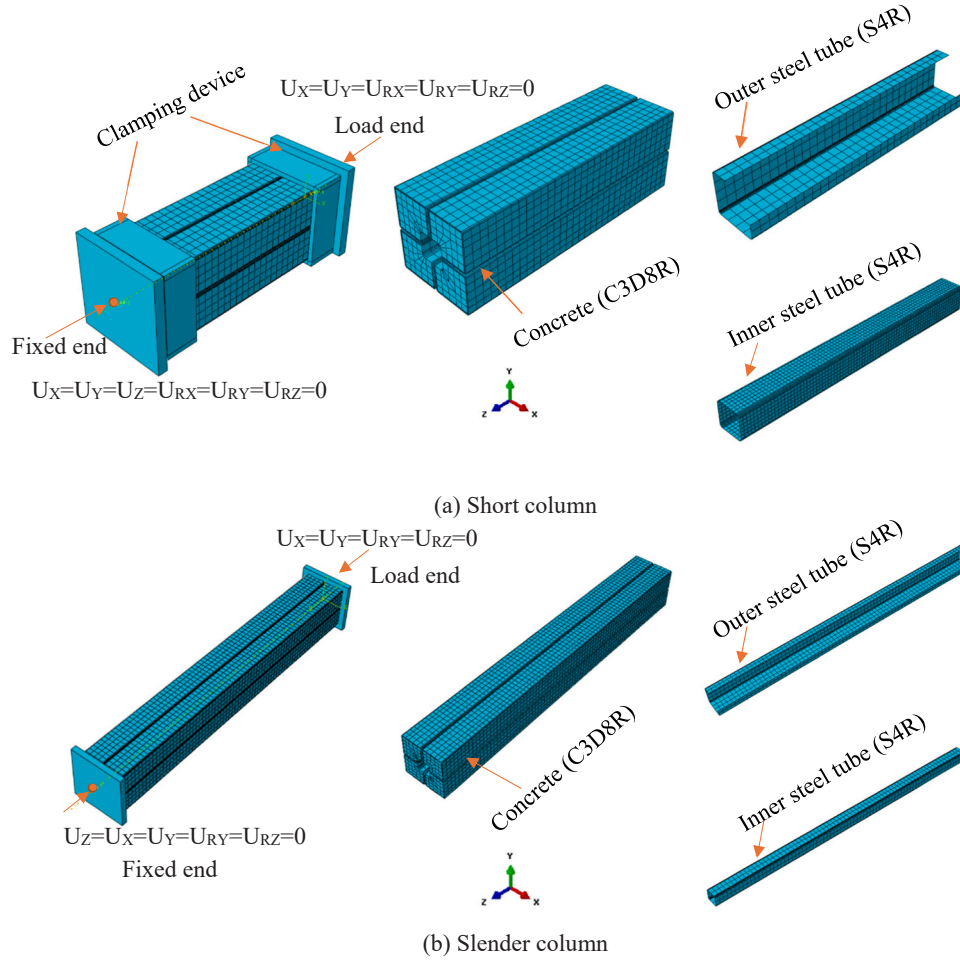| Group	Specimens	B_o(mm)	t_o(mm)	f_{yo}(MPa)	f_{cu}(MPa)	B_i(mm)	t_i(mm)	f_{yi}(MPa)	h_s(mm)	L_e(mm)	$\bar{\lambda}$	$N_{ul,Exp}$ (kN)	$N_{ul,FE}(f_c')$ (kN)	$\frac{N_{ul,FE}(f_c')}{N_{ul,Exp}}$	$N_{ul,FE}(f_{cc})$ (kN)	$\frac{N_{ul,FE}(f_{cc})}{N_{ul,Exp}}$
1 [45]	SS–160–1	160	1.9	293.9	50.2	50	2.76	331	30	480	0.13	1727.6	1588.7	0.92	1815.5	1.05
	SS–160–2	160	1.9	293.9	53.7	50	2.83	331	30	480	0.13	1884.4	1667.2	0.88	1913.7	1.02
	SS–160–3	160	1.9	293.9	87.6	50	2.83	331	30	480	0.15	2858.8	2354.7	0.82	2583.0	0.90
	SS–160–4	160	1.9	293.9	50.2	60	2.74	335.2	30	480	0.13	1722.9	1583.8	0.92	1770.3	1.03
	SS–160–5	160	2.7	336.6	50.2	50	2.79	331	30	480	0.13	1916.4	1853.6	0.97	2206.5	1.15
	SS–160–6	160	2.7	336.6	50.2	60	2.75	335.2	30	600	0.16	1905.4	1828.9	0.96	2145.0	1.13
2 [45]	SS–200–1	200	1.9	293.9	50.2	50	2.83	331	30	600	0.13	2338.4	2211.3	0.95	2483.7	1.06
	SS–200–2	200	1.9	293.9	53.7	50	2.78	331	30	600	0.13	2303.0	2385.5	1.04	2691.5	1.17
	SS–200–3	200	1.9	293.9	74.3	50	2.84	331	30	600	0.14	3037.4	3004.5	0.99	3351.7	1.10
	SS–200–4	200	1.9	293.9	87.6	50	2.80	331	30	600	0.15	3312.6	3494.1	1.05	3809.8	1.15
	SS–200–5	200	1.9	293.9	50.2	60	2.77	335.2	30	600	0.13	2359.0	2260.1	0.96	2554.1	1.08
	SS–200–6	200	2.7	336.6	50.2	50	2.76	331	30	600	0.13	2407.9	2593.8	1.08	3006.7	1.25
	SS–200–7	200	2.7	336.6	50.2	60	2.73	335.2	30	600	0.13	2655.5	2573.4	0.97	2976.0	1.12
3 [53,54]	S-C2-AM-L2	200	3.8	335.3	63.8	140	2.7	387.1	-	1640	0.35	3409	3262	0.96	3713	1.09
	CFST1	300 × 100	6.0	243.0	49.6	-	-	-	-	2500	1.23	2213	2147.2	0.97	2807	1.27
Mean														0.96		1.10
COV														0.068		0.083

(a) Short column

(b) Slender column

Fig. 7. Mesh configurations of short columns and slender columns.

of axial load–deflection responses obtained numerically from the FE model and from experimental results, along with the consistency in predicted failure modes, demonstrates that the model using f_c' yields more accurate predictions of the ultimate strength, deformation behaviour, and failure mechanisms of the composite columns.

3. Analysis of the behaviour of CFD-SSST slender columns

It is important to note the usual relationship between strength N and slenderness λ for axially-loaded columns, as illustrated in Fig. 11 [55]. The definition of λ follows the formula in Eq. 11 [55], where L_e is the effective buckling length, I_{DS} is the CFD-SSST section's second moment of area, and A_{DS} is the cross-sectional area. As can be seen in the figure, the plastic, inelastic, and elastic buckling stages are the three different failure phases. As illustrated in Fig. 11, λ_r is a limiting slenderness ratio that divides slender columns into long columns that fail because of elastic buckling and intermediate-length columns that fail because of inelastic buckling. This method for distinguishing between inelastic and elastic failure modes of CFST slender columns was adopted by DBJ/T13–51–2010 [56], where $\lambda_r = 115/(f_y/235)^{0.5}$.

$$\lambda = \frac{L_e}{\sqrt{I_{DS}/A_{DS}}} \tag{11}$$

Using the validated FE model, parametric studies were carried out to study the behaviour of the CFD-SSST slender columns with various properties, due to the limited number of available experimental tests. Seventy six FE were analysed. The parameters considered are the hollow ratio, the width-to-thickness ratio of the outer and inner steel tubes, the

depth of the stiffeners, the yield strength of the steel tubes, the strain distribution at the mid-height, confinement pressure, and the yield strength of the outer and inner steel tubes. Table 2 lists the details as well as the outcomes regarding the strengths ($N_{ul,FE}$) derived from the FE models. The slenderness ratios in groups G1–G3 were varied with cross-sectional widths ranging from 0.3 to 2.3. With varying parameters, the members of G4 and G5 are classified as intermediate-length columns and long columns, respectively. The non-dimensional slenderness ($\bar{\lambda} = \sqrt{N_{pl,Rk}/N_{cr}}$), displayed in Table 2, is calculated following EC4 [57], where $N_{pl,Rk}$ and N_{cr} are the plastic and critical resistances, respectively.

3.1. Column slenderness

It is evident that the slenderness of columns is a highly significant parameter, with more slender members generally exhibiting a greater influence from second order (P-Δ) effects. Fig. 12(a) shows the relationship between λ and the ultimate strength ($N_{ul,FE}$). As predicted, it is evident that as the slenderness ratio increases, the ultimate strength of CFD-SSST slender columns decreases. As the slenderness ratio rises, so does the effectiveness of employing various B_o values to increase the ultimate strength of columns. Conversely, the normalised strength versus λ relationships shown in Fig. 12(b) suggest that the columns with varying cross-section sizes exhibit comparable behaviour.

The relationships between mid-height deflection and ultimate axial load for CFD-SSST slender columns are shown in Fig. 13. This indicates that for intermediate-length columns, the load abruptly decreases when the concrete reaches the crushing strain, whereas for CFD-SSST slender columns, the post-strength becomes more stable as the slenderness ratio
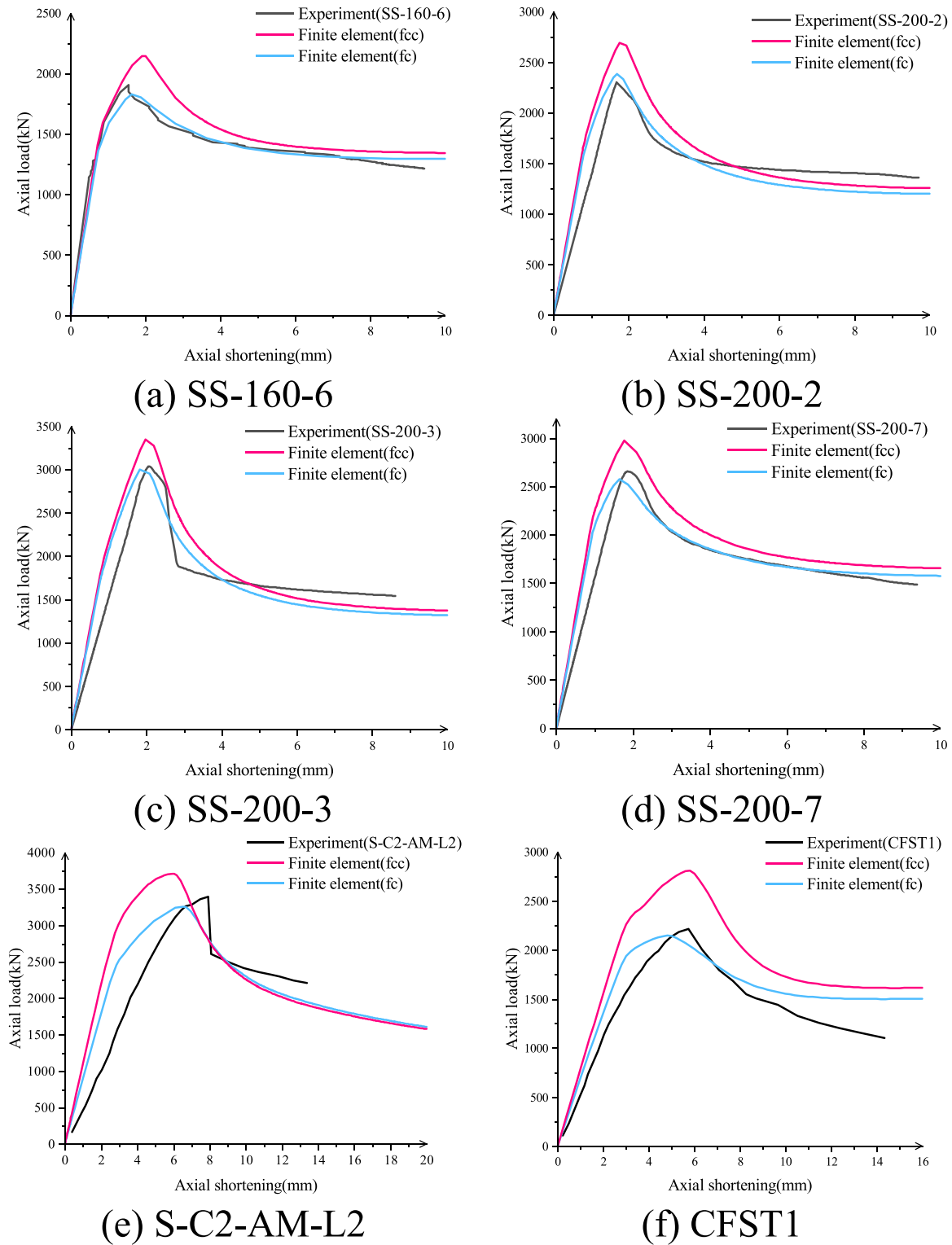
(a) SS-160-6

(b) SS-200-2

(c) SS-200-3

(d) SS-200-7

(e) S-C2-AM-L2

(f) CFST1

Fig. 8. Comparison of the axial load *versus* deflection responses obtained numerically from the FE model and from the experiments.

increases. However, in the design of tower and building structures, nonlinear and significant lateral displacement should be avoided.

3.2. Strain distribution at the mid-height

To distinguish between intermediate-length and long CFD-SSST slender columns, the relationships between ultimate axial load and longitudinal strain (ε_l) for columns S14 and S18 were analysed. The findings are shown in Fig. 14. Negative and positive values on the x-axis represent compressive and tensile strains. Looking at Fig. 14, it can be seen that both the outer and inner tubes of column S14 (L_e=4.8 m) are compressed until they reach the ultimate load. The longitudinal compressive strain at the ultimate strength is higher than the yield strain (=1119 $\mu\varepsilon_{lc}$) of the outer tube, indicating that the outer tube yielded before reaching the ultimate load. Therefore, it can be concluded that inelastic buckling occurred in S14. On the contrary, the outer tube of
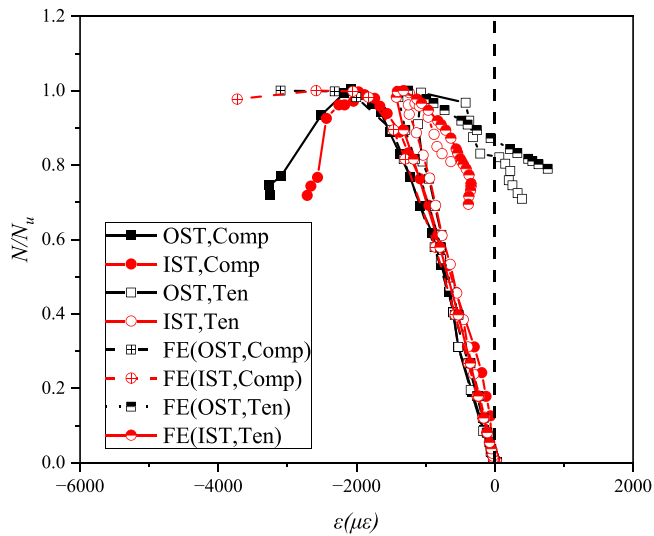
Fig. 9. Strain distribution comparisons between experiment and FE model for column S-C1-AM-L3 [54].

column S18 (L_e=8.4 m) is under tension before reaching the ultimate strength, and the longitudinal compressive strain at the ultimate strength is lower than the yield strain (=1119 $\mu\varepsilon_{lc}$) of the outer tube, suggesting that the full capacity of the outer tube is not fully utilised. Thus, it can be concluded that elastic buckling took place in S18.

Based on Fig. 11, S14 and S18 are defined as intermediate-length and long columns, respectively. The classification of other FE models can be seen in Table 3, where INB and EB stand for inelastic and elastic buckling behaviours. From Table 3, it can be observed that the critical slenderness ratio (λ_r) separating intermediate-length and long CFD-SSST columns is around λ_r about 110 when the yield stress of the outer tube is 235 MPa, equivalent to $\overline{\lambda} = 1.4$. This value is very close to the specified value of 1.5 by AISC-LRFD-99 [58] to distinguish between inelastic and elastic flexural buckling.

3.3. Confinement effect

It is acknowledged that it is extremely difficult to measure the lateral pressure applied to infilled concrete in concrete-filled tubular specimens
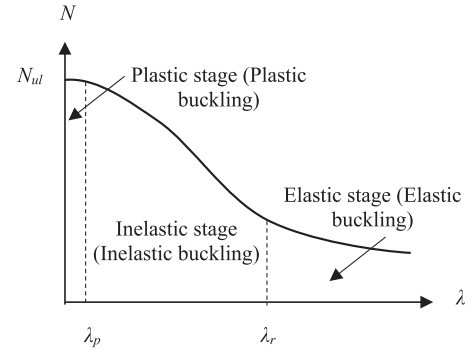
Fig. 11. Column strength *versus* slenderness ratio relationship [55].

(a) SS-160-5 [45]

(b) SS-200-2 [45]

(c) S-C2-AM-L2 [54]

(d) CFST1 [53]
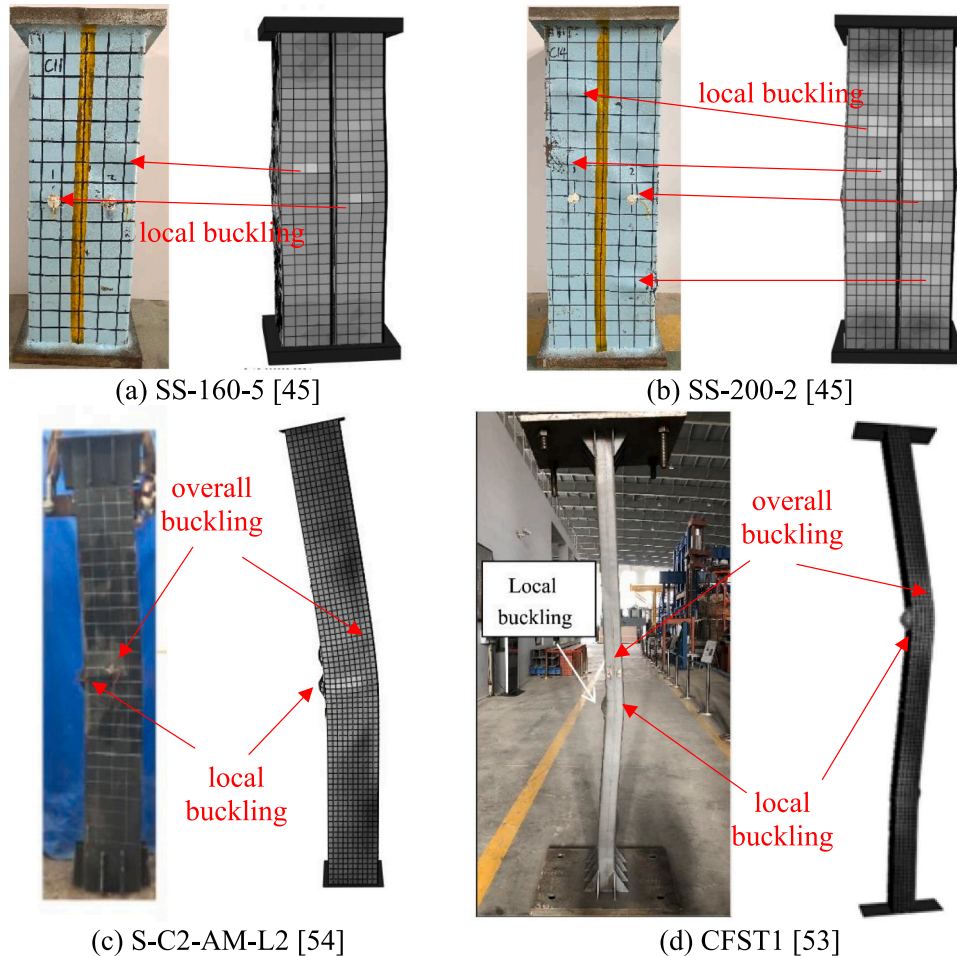
Fig. 10. Comparison of failure modes from FE models and tests [45,53,54].

Table 2
Details and results from the parametric study on CFD-SSST columns.

| Group	FE model	B_o (mm)	t_o (mm)	B_o/t_o	f_{cs} (MPa)	f_{yo} (MPa)	h_s (mm)	B_i (mm)	t_i (mm)	B_i/t_i	f_{yi} (MPa)	B_i/B_o	L_e (mm)	λ	$\bar{\lambda}$	$N_{ul,FE}$ (kN)
G1	S1	160	2	80	40	235	20	80	3	27	355	0.5	1200	23.2	0.29	1263
	S2												2700	52.3	0.66	1043
	S3												3600	69.7	0.88	909
	S4												4200	81.3	1.03	817
	S5												5400	104.6	1.32	631
	S6												6000	116.2	1.47	549
	S7												6600	127.8	1.62	476
	S8												7200	139.4	1.76	410
	S9												7800	151.0	1.91	342
	S10												9000	174.3	2.21	265
G2	S11	180	2	90	40	235	30	80	3	27	355	0.44	1500	26.4	0.33	1462
	S12												3000	52.8	0.66	1266
	S13												3900	68.6	0.86	1144
	S14												4800	84.4	1.06	991
	S15												5700	100.2	1.26	836
	S16												6900	121.3	1.53	621
	S17												7500	131.9	1.66	547
	S18												8400	147.7	1.86	465
	S19												9000	158.3	1.99	407
	S20												10000	175.9	2.22	330
G3	S21	280	2	140	40	235	35	80	3	27	355	0.29	2100	25.0	0.31	3226
	S22												4200	50.0	0.63	2798
	S23												6300	74.9	0.94	2342
	S24												7800	92.8	1.16	1962
	S25												9000	107.1	1.34	1677
	S26												9900	117.8	1.48	1476
	S27												12000	142.7	1.79	1087
	S28												13000	154.6	1.94	943
	S29												14000	166.5	2.09	818
	S30												15000	178.4	2.24	716
G4: intermediate-length columns	S31	180	2	90	40	235	30	80	3	27	355	0.44	4800	84.4	1.06	991
	S32		2	90	40	355	30	80	3	27	355	0.44		84.4	1.14	1099
	S33		2	90	40	420	30	80	3	27	355	0.44		84.4	1.17	1139
	S34		2	90	40	460	30	80	3	27	355	0.44		84.4	1.20	1153
	S35		2	90	50	235	30	80	3	27	355	0.44		84.4	1.10	1086
	S36		2	90	60	235	30	80	3	27	355	0.44		84.4	1.14	1181
	S37		2	90	70	235	30	80	3	27	355	0.44		84.4	1.18	1265
	S38		2	90	80	235	30	80	3	27	355	0.44		84.4	1.21	1349
	S39		2	90	40	235	30	80	3	27	235	0.44		84.4	1.03	987
	S40		2	90	40	235	30	80	3	27	420	0.44		84.4	1.08	987
	S41		2	90	40	235	30	80	3	27	460	0.44		84.4	1.10	987
	S42		2	90	40	235	10	80	3	27	355	0.44		84.4	1.07	947
	S43		2	90	40	235	20	80	3	27	355	0.44		84.4	1.06	961
	S44		2	90	40	235	40	80	3	27	355	0.44		84.4	1.07	1005
	S45		2	90	40	235	30	60	3	20	355	0.33		87.6	1.08	991
	S46		2	90	40	235	30	90	3	30	355	0.5		82.6	1.05	989
	S47		2	90	40	235	30	100	3	33	355	0.56		80.8	1.04	983
	S48		2.5	72	40	235	30	80	3	27	355	0.44		84.4	1.04	1066
	S49		3	60	40	235	30	80	3	27	355	0.44		84.4	1.01	1139
	S50		4	45	40	235	30	80	3	27	355	0.44		84.4	0.98	1281
	S51		2	90	40	235	30	80	2	40	355	0.44		84.4	1.04	989
	S52		2	90	40	235	30	80	4	20	355	0.44		84.4	1.09	1021
	S53		2	90	40	235	30	80	5	16	355	0.44		84.4	1.11	1066
G5: long columns	S54	180	2	90	40	235	30	80	3	27	355	0.44	7500	147.7	1.86	463
	S55		2	90	40	355	30	80	3	27	355	0.44		147.7	1.99	464
	S56		2	90	40	420	30	80	3	27	355	0.44		147.7	2.05	464
	S57		2	90	40	460	30	80	3	27	355	0.44		147.7	2.09	464
	S58		2	90	50	235	30	80	3	27	355	0.44		147.7	1.93	500
	S59		2	90	60	235	30	80	3	27	355	0.44		147.7	2.00	533
	S60		2	90	70	235	30	80	3	27	355	0.44		147.7	2.06	564
	S61		2	90	80	235	30	80	3	27	355	0.44		147.7	2.12	592
	S62		2	90	40	235	30	80	3	27	235	0.44		147.7	1.79	464
	S63		2	90	40	235	30	80	3	27	420	0.44		147.7	1.90	464
	S64		2	90	40	235	30	80	3	27	460	0.44		147.7	1.92	464
	S65		2	90	40	235	10	80	3	27	355	0.44		131.9	1.66	447
	S66		2	90	40	235	20	80	3	27	355	0.44		131.9	1.66	456
	S67		2	90	40	235	40	80	3	27	355	0.44		131.9	1.67	469
	S68		2	90	40	235	30	60	3	20	355	0.33		136.9	1.68	458
	S69		2	90	40	235	30	90	3	30	355	0.5		129.1	1.64	467
	S70		2	90	40	235	30	100	3	33	355	0.56		126.2	1.62	472
	S71		2.5	72	40	235	30	80	3	27	355	0.44		131.9	1.62	507
	S72		3	60	40	235	30	80	3	27	355	0.44		131.9	1.58	546
	S73		4	45	40	235	30	80	3	27	355	0.44		131.9	1.53	624

Table 2 (*continued*)

Group	FE model	B_o (mm)	t_o (mm)	B_o/t_o	f_{cs} (MPa)	f_{yo} (MPa)	h_s (mm)	B_i (mm)	t_i (mm)	B_i/t_i	f_{yi} (MPa)	B_i/B_o	L_e (mm)	λ	$\bar{\lambda}$	$N_{ul,FE}$ (kN)
	S74		2	90	40	235	30	80	2	40	355	0.44		131.9	1.62	458
	S75		2	90	40	235	30	80	4	20	355	0.44		131.9	1.70	452
	S76		2	90	40	235	30	80	5	16	355	0.44		131.9	1.74	474

(a)

(b)
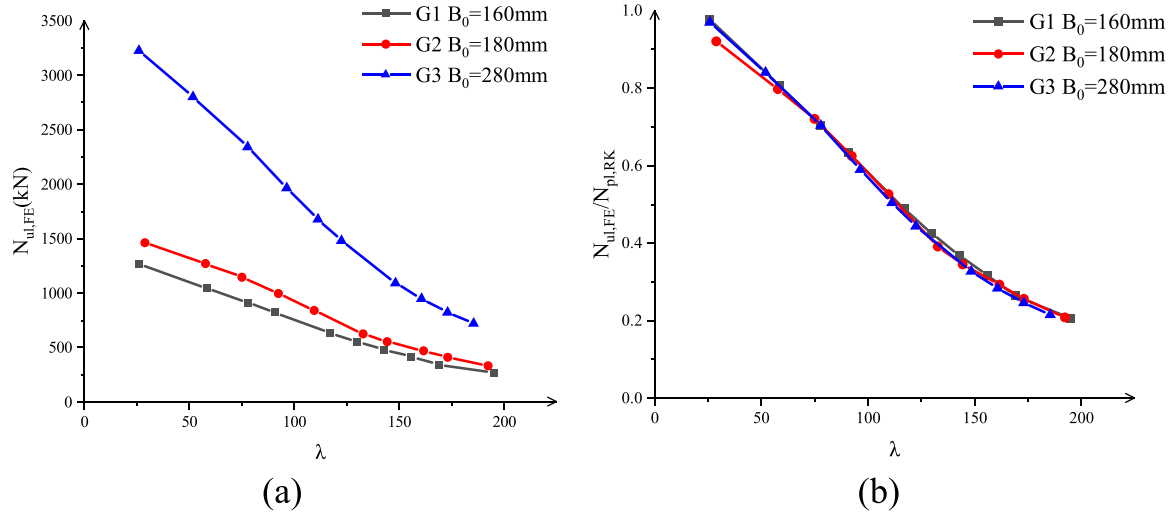
Fig. 12. Effect of slenderness ratio λ on the (a) ultimate strength and (b) normalised ultimate strength of CFD-SSST columns.

(a) B_o=160mm

(b) B_o=180mm

(c) B_o=280mm
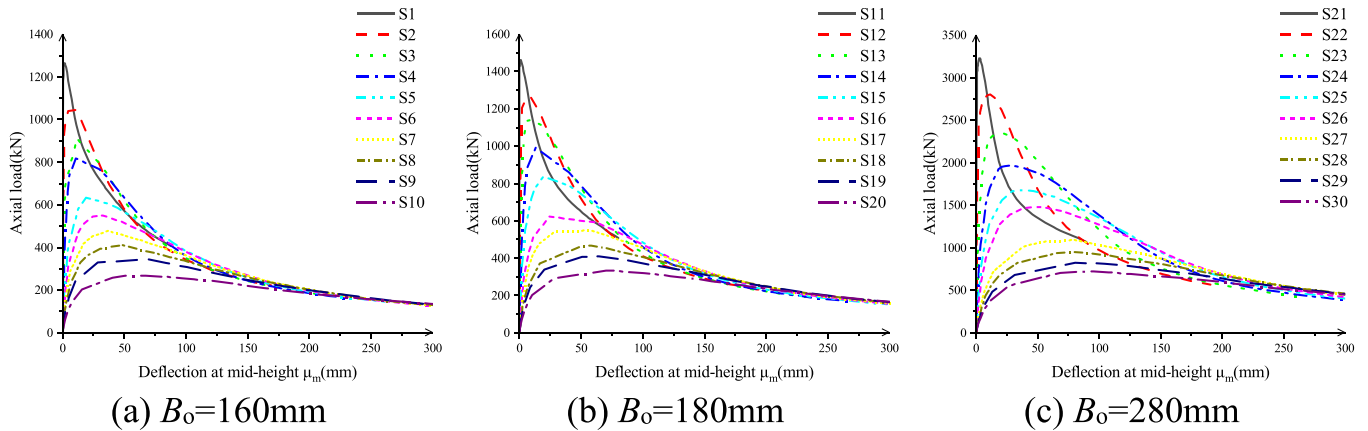
Fig. 13. Load-lateral displacement relationships for CFD-SSST columns.

based solely on experimental data. Since ε_h and ε_{lc} are the hoop and longitudinal strains, respectively, in the steel tubes at the mid-height at the centre of the flat fold of the tubes, the relationships between ultimate axial load and $\varepsilon_h/\varepsilon_{lc}$ are thus investigated in this section. The results for the group G1 specimens are shown in Fig. 15. The steel tube is usually in a uniaxial stress state for columns with an outer width of B_o= 160 mm when the value of $\varepsilon_h/\varepsilon_{lc} \leq 0.3$ (higher than the concrete's Poisson's ratio, which normally equals 0.2). Because the dilation of the sandwiched concrete is less than that of the steel tube under the same axial deformation, the effect of confinement is therefore minimal in this instance.

The concrete dilates laterally as the applied load rises. The results for columns S1 to S5 demonstrate that when the axial load reached 60–100 % of the column strength, the values of $\varepsilon_h/\varepsilon_{lc}$ for many specimens increased considerably above their initial values. Given that the dilation was limited by the outer steel tube, this implies that the sandwiched concrete is subject to confining pressures. The confinement ef-

fect of the outer tube on the infilled concrete is inversely proportional to the column length, as shown by Fig. 15(a), where the value of $\varepsilon_h/\varepsilon_{lc}$ at ultimate axial load decreases as column length increases. This is due to the fact that secondary bending moments rise as column length increases [43]. The inner steel tube was restrained and shielded by the outer tube and sandwiched concrete, as shown by Fig. 15(b), where the value of $\varepsilon_h/\varepsilon_{lc}$ in the early loading stages is less than 0.3 (roughly ranging between 0.26 and 0.30). When $\varepsilon_h/\varepsilon_{lc} \geq 0.3$, the core concrete is confined as the load increases. Note that changing the column width (B_o=180 mm and B_o =280 mm) also yields similar results.

Another interesting finding is that, in contrast to the core concrete (inside the inner tube only), the positive effect of confinement starts earlier in the response for the sandwiched concrete (i.e., between the inner and outer steel tubes). The outer steel tube effectively restrains the sandwiched concrete, and the hoop stresses in the outer steel become tensile as the load increases and the compressed sandwiched concrete starts to behave plastically. The lateral deformations in the sandwiched
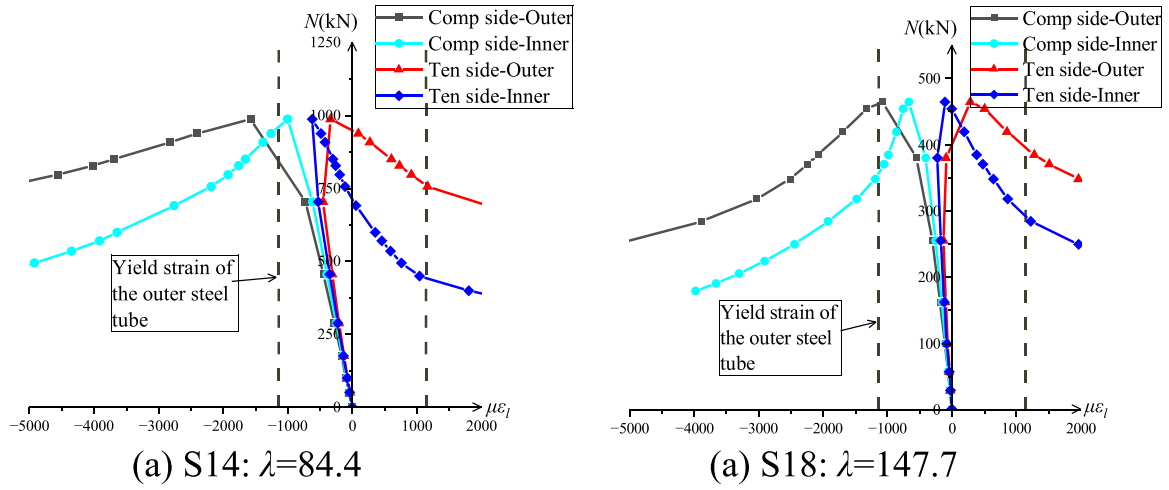
(a) S14: λ=84.4

(a) S18: λ=147.7

Fig. 14. Load-longitudinal strain (ε_{lc}) relationship for typical CFD-SSST columns.

Table 3
Inelastic and elastic failure modes for the CFD-SSST columns.

G1	λ	23.2	52.3	69.7	81.3	104.6	116.2	127.8	139.4	151.0	174.3
	Failure mode	**INB**	**INB**	**INB**	**INB**	**INB**	**EB**	**EB**	**EB**	**EB**	**EB**
G2	λ	26.4	52.8	68.6	84.4	100.2	121.3	131.9	147.7	158.3	175.9
	Failure mode	**INB**	**INB**	**INB**	**INB**	**INB**	**EB**	**EB**	**EB**	**EB**	**EB**
G3	λ	25.0	50.0	74.9	92.8	107.0	117.8	142.7	154.6	166.5	178.4
	Failure mode	**INB**	**INB**	**INB**	**INB**	**INB**	**EB**	**EB**	**EB**	**EB**	**EB**

(a) Outer steel tube
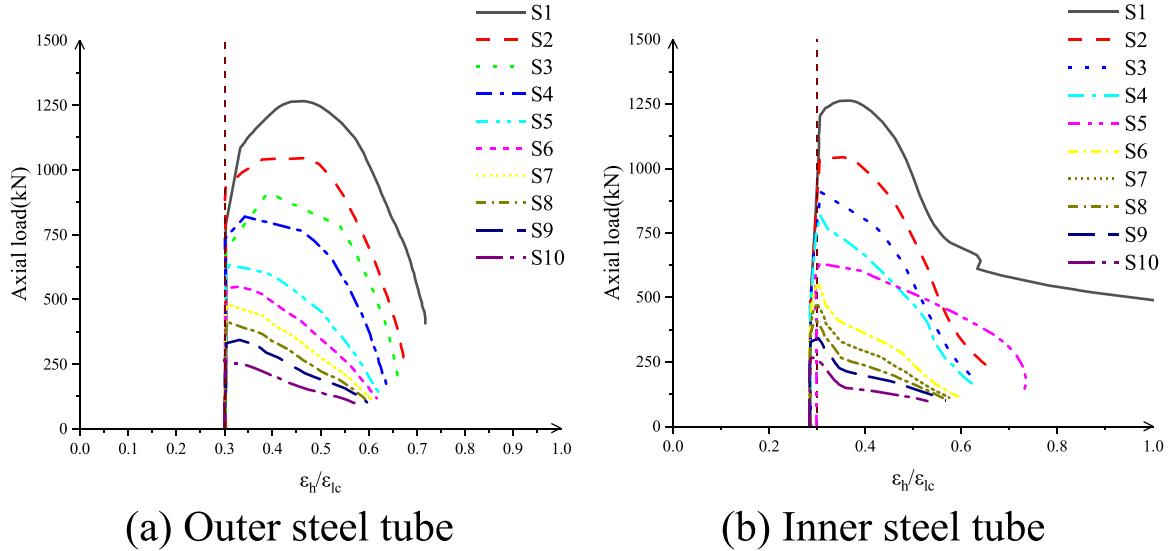
(b) Inner steel tube

Fig. 15. Load *versus* $\varepsilon_h/\varepsilon_{lc}$ for CFD-SSST columns in G1 (B_o=160 mm).

concrete are comparable to those in the outer steel. The steel tube is in a biaxial stress state at this point and for the duration of the response, while the sandwiched concrete is under a triaxial stress state.

For long columns only (S6-S10 for columns of B_o=160 mm), the sandwiched concrete is compressed triaxially when the load reaches the final column load; however, for intermediate-length columns (S1 to S5), the confinement of the sandwiched concrete begins earlier, in the ascending branch of the load-lateral displacement relationships (i.e. 60–90 % of the column strength). The lateral deformation of the inner steel tube increases with increasing levels of axial stress because the pressure on the inner tube decreases as the sandwiched concrete dilates with increasing load.

Moreover, a confinement analysis has been carried out to clarify the effect of column's slenderness ratio on the contact stress between the sandwiched concrete and the outer steel tube especially at the corner regions of the cross section. As shown in Fig. 16, increasing the slenderness ratio decreases the contact stress at various B_o/t_o ratios. This effect is remarkable in the columns with higher ratios of B_o/t_o.

The concrete stress distribution in the cross-section at the mid-height for varying load levels is displayed in Fig. 17 using columns S37 and S60 to illustrate the response of intermediate-length and long columns, respectively. In each image, the black horizontal line between the compressive and tensile regions shows the location of the neutral axis. As can be noticed, the neutral axis moves in closer proximity to the
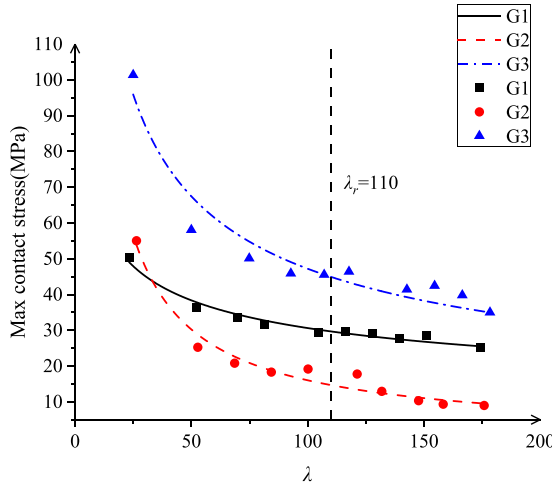
Fig. 16. Effect of slenderness on confinement of CFD-SSST slender columns.

cross-sectional centroid as load increases.

### 3.4. Influence of the inner tube and core concrete

The influence of the inner tube and core concrete on the ultimate axial strength and behaviour of CFD-SSST slender columns is currently considered through comparing the CFD-SSST slender columns with CFSST and CFDSST columns, as seen in Table 4. The CFSST column is that provided in Fig. 1(d), while CFDSST column is typical to CFD-SSST columns but with additional concrete core. Herein, intermediate-length column S14 and long column S18 were considered to accomplish the comparative study between these different cross-sections. The material and geometric properties of these columns, along with their strength, are shown in Table 4. Moreover, the weights (W_T) of the columns were calculated to obtain the optimum cross-section among the three types,

through obtaining the strength-to-weight (S/W_T) ratio (i.e. N_{FE}/W_T). The values of W_T are the total weights of columns, which are the sum of the weights of concrete and steel. Note that the members' weight calculations were based on the cubic meter self-weights of steel and plain concrete, which were determined to be 7850 kg/m³ and 2400 kg/m³, respectively.

For both cases of intermediate-length and slender columns, the resistances of CFDSST columns are the most compared to CFD-SSST and CFSST columns, simply because the cross-section uses both the inner tube and concrete core. CFSST columns, on the other hand, have the less S/W_T ratio than CFD-SSST columns, indicating that cost and safety are not balanced. While the strength of CFD-SSST columns is 93 % of that of CFDSST columns, for both column lengths, the former own much higher S/W_T ratios. This ensures that using CFD-SSST columns provides the best balance between cost and safety for the considered cross-sections. In case of slender columns, it can also be noted that the S/W_T ratio of the CFD-SSST column is higher than that of CFSST column, despite having less axial resistance. Note that for slender columns, filling the entire cross-section with concrete becomes more efficient than adding an inner steel tube. This is because the concrete, as a rigid medium, contributes more in the flexural stiffness of the slender column (i.e. those fail elastically).

The FE axial strength and lateral displacement at mid-height of the CFD-SSST slender columns are compared to those of their counterparts in Fig. 18. It is evident that intermediate-length columns have a higher strength efficiency increase than long columns. For intermediate-length columns, the inner steel tube's role in supporting applied load and enhancing the section's flexural stiffness is more noticeable than for longer members. Conversely, flexural stiffness is more important than material strength when long columns fail due to elastic buckling. Since double-skin composite members use less material while having load capacities comparable to those of CFSST and CFDSST columns, they offer a better solution for the parameters investigated in this study.

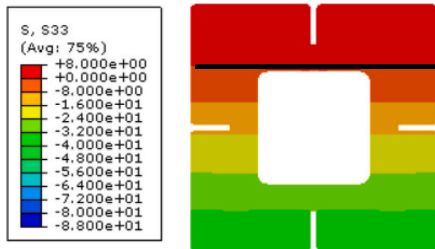Initiation of confinement in sandwiched concrete also approximately at $N_{ul,FE}$(N=1265 kN)
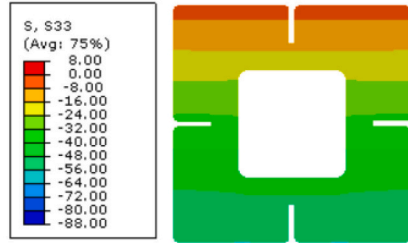
88.6% $N_{ul,FE}$ in descending branch (N=1121 kN)

(a) S37
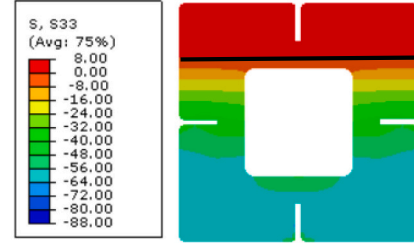
Initiation of confinement in the sandwiched concrete also approximately at $N_{ul,FE}$ (N=564 kN)
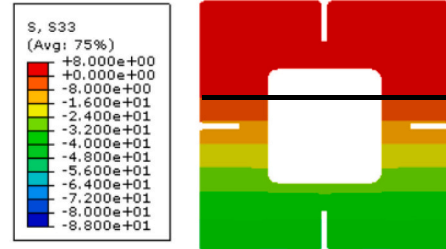
92.4% $N_{ul,FE}$ in descending branch (N=521 kN)

(b) S60
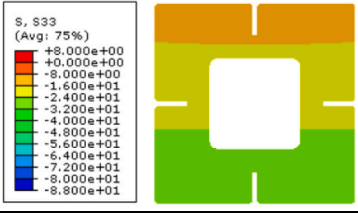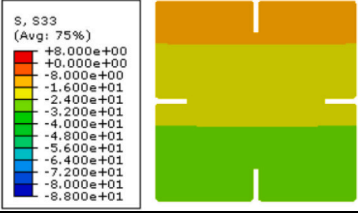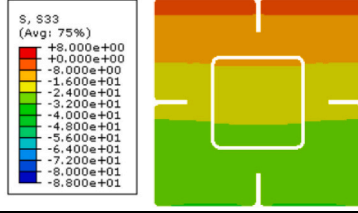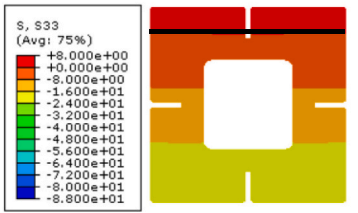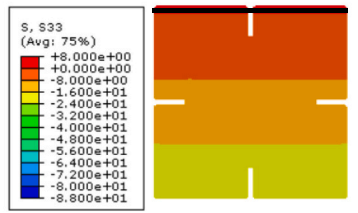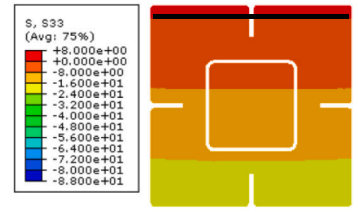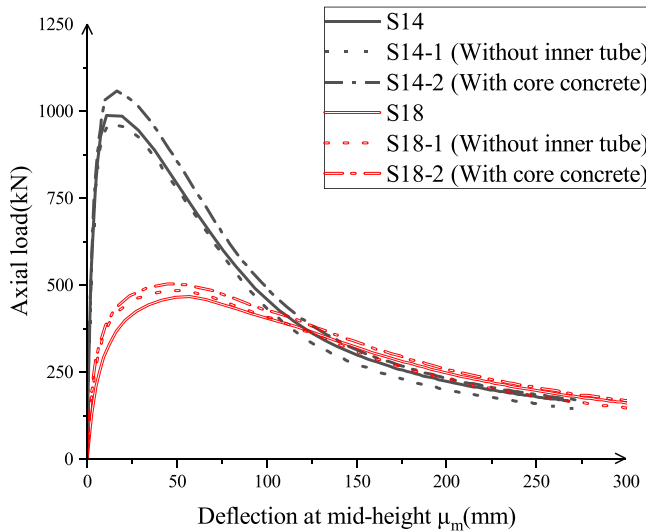
Fig. 17. Stress distribution in the infill concrete for (a) intermediate-length and (b) long columns.

Table 4
Comparison between CFD-SSST slender columns and their counterparts formed without inner tube or concrete.

Column type	CFD-SSST	CFSST	CFDSST
(a) Intermediate-length columns – S14			
Stress contour of concrete			
N_{FE} (kN)	991	964	1059
*Weight (*kN)	3.76	4.14	4.38
S/W_T	**264**	**233**	**242**
(b) Long columns – S18			
Stress contour of concrete			
N_{FE} (kN)	465	482	502
*Weight (*kN)	6.58	7.25	7.66
S/W_T	**71**	**66**	**66**

Fig. 18. Comparison between the axial load *versus* lateral displacement relationships at mid-height of CFD-SSST slender columns with different composite configurations.

3.5. Strength of steel material

Fig. 19 displays the results of the analysis regarding the steel strength, which varied the outer and inner tubes to yield strengths of 235, 355, 420, and 460 MPa. The impact of varying steel tube yield strengths on ultimate strength in relation to lateral displacement at mid-height is depicted in Fig. 20. Referring to Fig. 19, it can be seen that while the long columns are not significantly affected, the ultimate strength of CFDSST intermediate-length columns increases corresponding to the increase in the outer steel tube's yield strength. For instance, between S31 and S34, the outer steel tube yield strength rose from 235 MPa to 460 MPa, resulting in a 16.3 % increase in load capacity. Furthermore, this analysis demonstrates that the yield strength of the inner steel tube has a negligible impact. However, as can be seen from Fig. 19(b), increasing yield strength lowers the columns' $N_{ul,FE}/N_{pl,Rk}$ ratios, indicating decreased efficiency linked to an increase in f_y values. This is further corroborated by the normalised strength-deflection relationships displayed in Fig. 20(b). Furthermore, the effect of yield strength of the outer steel tube has been studied at various concrete compressive strengths as shown in Fig. 21. For intermediate length columns, the outer tube's yield strength has a considerable effect by 17.5 % increase (at average) in the ultimate load at all concrete grades. However, for long columns, the effect of outer tube's material yield strength has no effect on the ultimate load.

3.6. Strength of sandwiched concrete

By adjusting the values between 40 and 80 MPa, the impact of the sandwiched concrete's (f_{cs}) strength was evaluated; the outcomes are shown in Fig. 22. Fig. 23 illustrates how varying concrete strengths affect the ultimate strength in relation to lateral displacement at the mid-height. The ultimate strength of CFD-SSST intermediate-length columns is found to increase significantly when the sandwiched concrete strength is increased (e.g., 36.1 % increase in strength by increasing f_{cs}
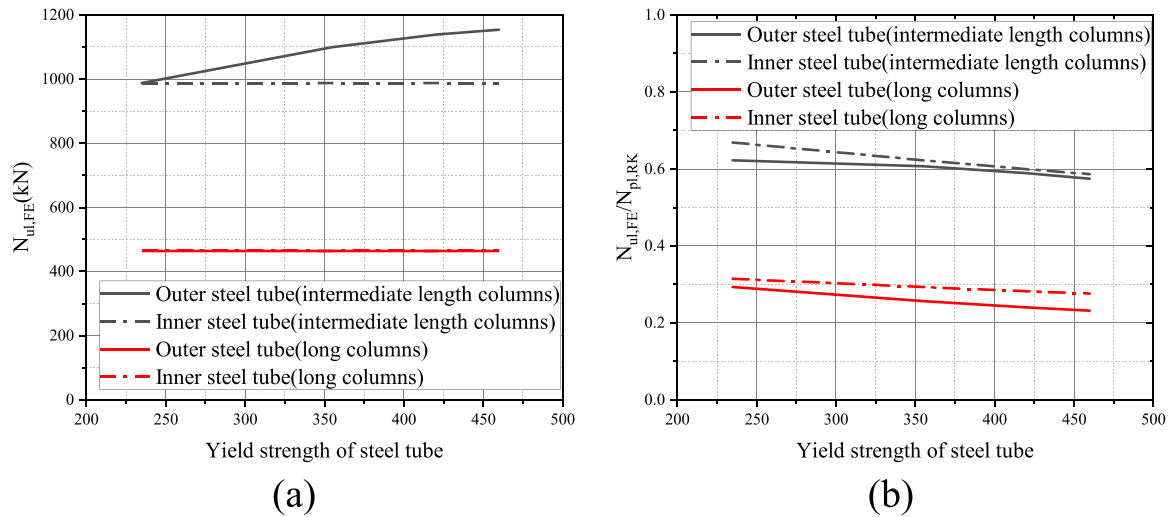
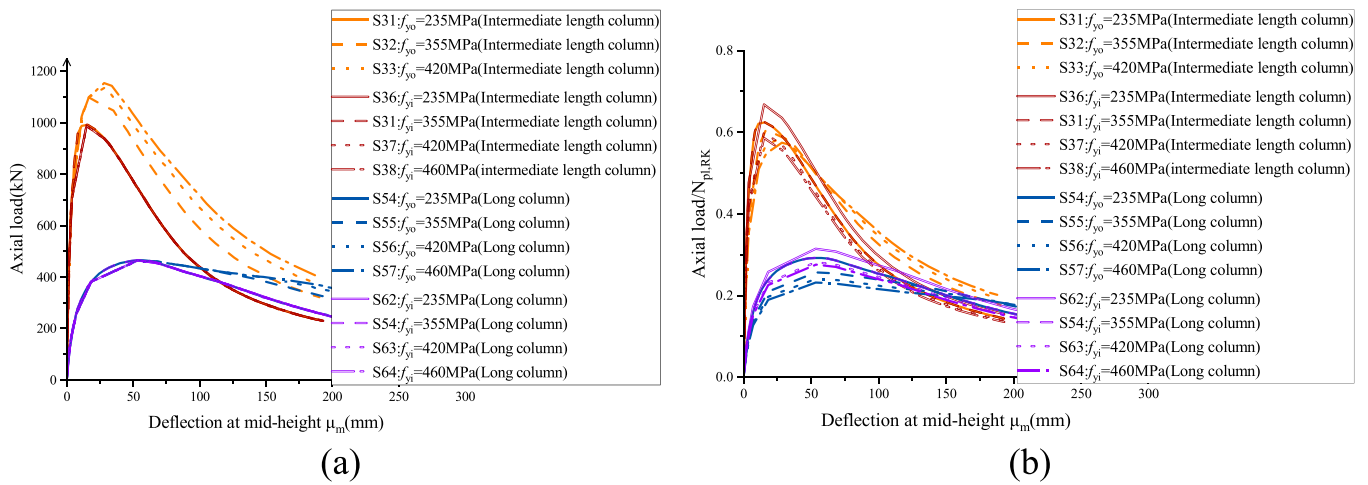**Fig. 19.** Influence of steel yield strength values on the ultimate strength of CFD-SSST slender columns.

Fig. 20. Influence of steel yield strength on the axial load *versus* lateral displacement responses of CFD-SSST slender columns.
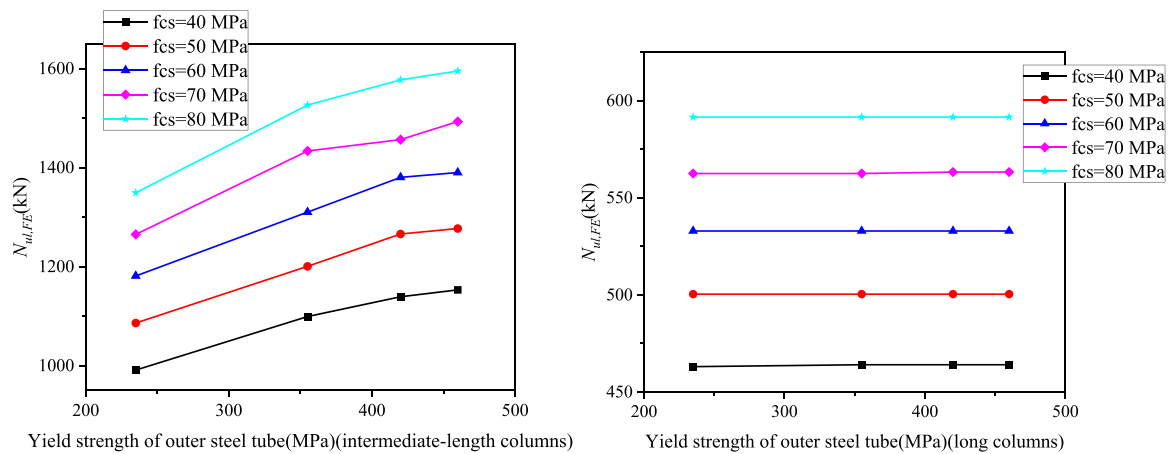

Fig. 21. Ultimate load *versus* yield strength of outer steel tube based on different concrete strengths.

from 40 to 80 MPa), whereas the effect is less significant but still noticeable for CFD-SSST long columns (e.g., 27.9 % increase in strength by increasing f_{cs} from 40 to 80 MPa). Again, the various failure modes are to reason of this discrepancy. It is evident from Fig. 23 that slender

columns exhibit enhanced ductility for higher concrete grades. However, as shown in Fig. 22(b), the columns' $N_{ul,FE}/N_{pl,Rk}$ ratios slightly decrease as concrete strength increases, suggesting that the increased f_c values are associated with decreased efficiency. The prior conclusion is
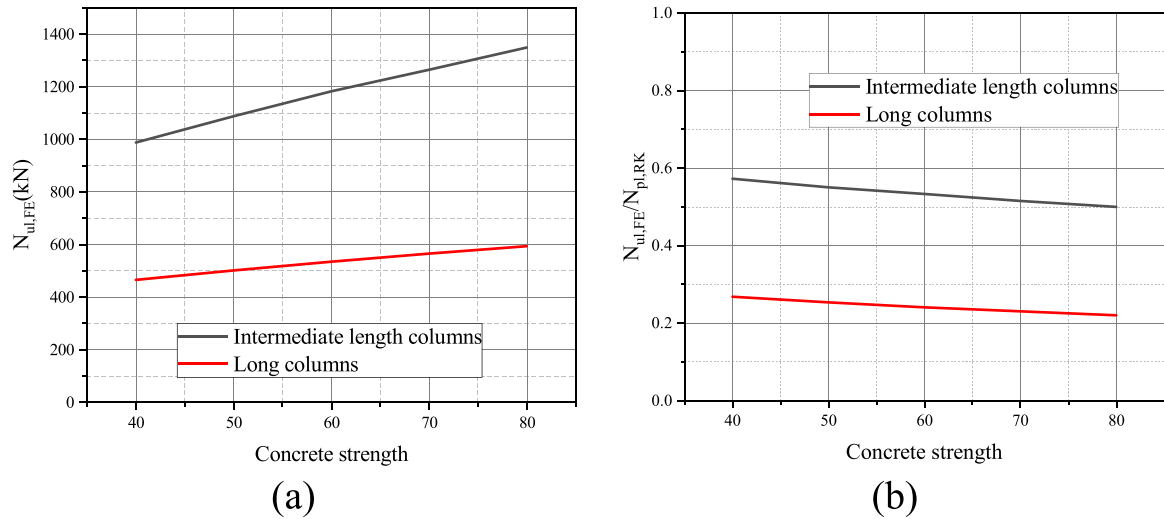
Fig. 22. Influence of different concrete strength values (in MPa) on the ultimate strength of CFD-SSST slender columns.
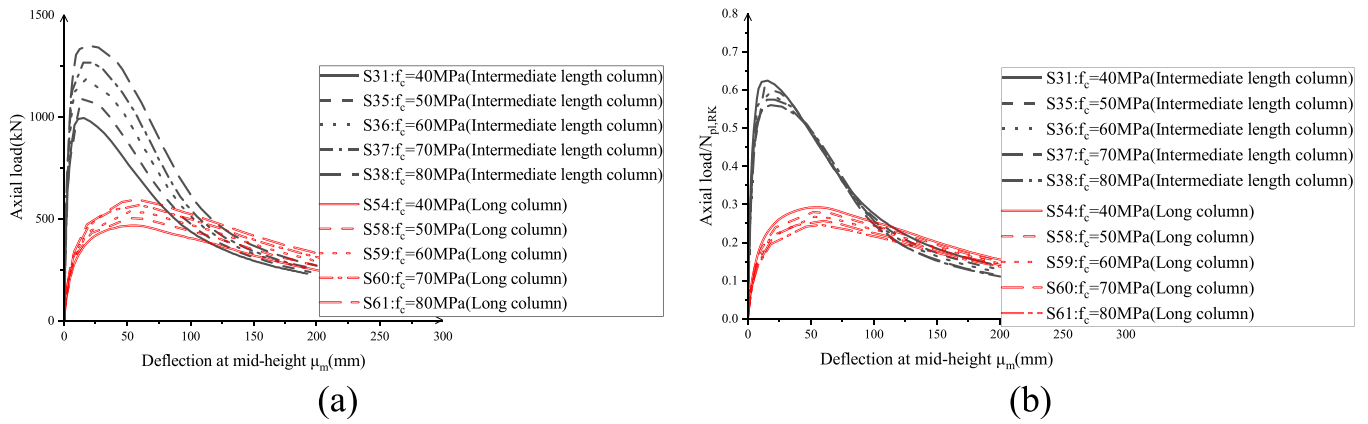

Fig. 23. Influence of different concrete strength values on the axial load *versus* lateral displacement responses of CFD-SSST slender columns.

supported by the impact of f_c values on the normalised strength-deflection relationships, as shown in Fig. 23(b).

3.7. Depth of stiffeners

Fig. 24(a) presents the effect of varying the stiffener depth (h_s) in the outer steel tubes, with values of 10, 20, 30, and 40 mm investigated. For different combinations of outer tube thickness (t_o) and yield strength
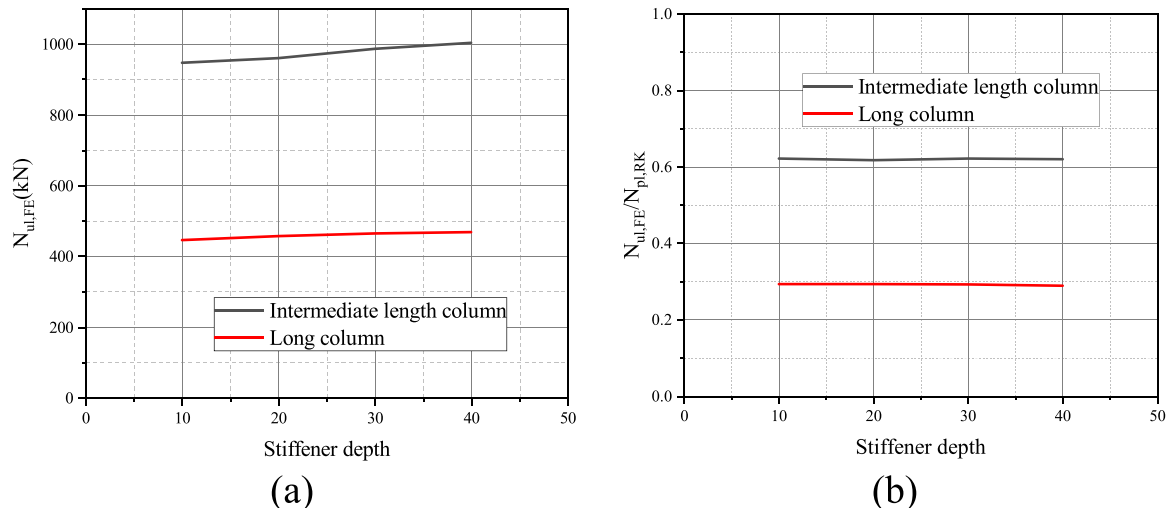

Fig. 24. Influence of different stiffener depths (in mm) on the ultimate strength of CFD-SSST slender columns.

(f_{yo}) as defined in Groups G2, G4, and G5 in Table 2, the minimum required stiffener depth $h_{s,min}$ for $B_o = 180$ mm is calculated to range from 17 to 25 mm using Eq. (23), in accordance with the recommendation by Tao et al. [10]. The ultimate strength of intermediate-length CFD-SSST columns is observed to increase with increasing stiffener depth, but this enhancement becomes negligible for $h_s > 30$ mm. In contrast, the ultimate strength and behaviour of long columns are largely insensitive to changes in stiffener depth. Despite Tao et al.'s assertion that the minimum stiffener depth as defined by Eq. (23) is generally adequate, the plots of normalised strength ($N_{ul,FE}/N_{pl,Rk}$) versus h_s shown in Fig. 24(b) display nearly flat trends. This indicates that variations in stiffener depth beyond the minimum required value have minimal influence on the normalised axial capacity of the columns.

$$h_{s,min} = \sqrt[3]{\frac{12 I_s}{2 t_o}}, \quad I_s = 3.1 \times 10^{-4} \left(\frac{0.5 B_o - 2 t_o}{t_o} \right) \frac{f_{yo}}{280} t_o^4 \quad (23)$$

3.8. Steel tubes' width-to-thickness ratio

The influence of the width-to-thickness ratios of the inner (B_i/t_i) and outer (B_o/t_o) steel tubes on the ultimate axial capacity is illustrated in Fig. 25. As shown in Fig. 25(a), increasing the B_i/t_i ratio has a negligible impact on the ultimate strength of CFD-SSST slender columns, whereas increasing the B_o/t_o ratio leads to a noticeable reduction in strength. However, this strength reduction is accompanied by a significant decrease in steel consumption. For example, increasing the B_o/t_o ratio from 45 to 72 in intermediate-length columns S50 and S48 results in a 16.8 % reduction in axial strength but a 37 % reduction in the cross-sectional area of the outer tube. Fig. 25(b) presents the relationship between width-to-thickness ratios and the normalised ultimate axial capacity ($N_{ul,FE}/N_{pl,Rk}$) for both inner and outer tubes. It is evident that increasing the slenderness of the inner steel tube section can slightly enhance the normalised strength for intermediate and long columns. In contrast, for the outer steel tube, the normalised strength appears to stabilise across the range of investigated B_o/t_o values. Additionally, Fig. 26 compares both the absolute and normalised strengths against mid-span deflection. It is observed that increasing the B_o/t_o ratio reduces the residual strength in the post-peak response, indicating a more brittle failure behaviour. On the other hand, variations in B_i/t_i do not significantly affect the residual strength in the post-peak range.

3.9. Hollow ratio

The hollow ratio χ is defined as the ratio of the inner to outer tube widths, B_i/B_o. The influence of χ on the ultimate axial capacity of CFD-SSST slender columns is presented in Fig. 27(a). The intermediate-length columns S45–S47 and the long columns S68–S70 encompass the studied range of hollow ratios, which varies from 0.33 to 0.56. In these models, the outer tube width B_o remains constant, while the inner tube width is adjusted to achieve the desired hollow ratio.

As observed in Fig. 27, increasing the hollow ratio χ has a minimal effect on the axial strength of both intermediate and long CFD-SSST columns. This observation is further supported by the normalised strength versus hollow ratio curves shown in Fig. 27(b), which demonstrate relatively flat trends. These results suggest that, within the range of parameters considered, adopting smaller values of χ leads to more structurally efficient designs. It is important to note that, due to the presence of stiffeners, the maximum achievable hollow ratio in CFD-SSST sections is constrained by ($B_o - 2h_s$)/B_o. Nevertheless, studies on other double-skin tubular columns—particularly those used in wind turbine towers—have explored much higher hollow ratios, up to 0.87 [59–61].

4. Design of CFD-SSST slender columns

The application of current design expressions for CFD-SSST slender columns to the columns of the current study was investigated with the necessary modifications made, as described below, because there are no design methods for the CFD-SSST slender columns. Because of the potential for local buckling of the thin-walled section, the ultimate strength of composite members is determined by the value of the outer tube's effective cross-sectional area ($A_{sy,eff}$) in compliance with Eurocode 3 Part 1–1 [62]. The critical load of thin columns for concrete-filled composite columns is determined by the column's effective length and flexural stiffness [43]. In this assessment, the reliability index β—a relative measure of design integrity used by other researchers [e.g. 63, 64]—is calculated as follows:

$$\beta = \frac{\mathrm{Ln}\left(\frac{N \bullet M \bullet F}{\Phi} \right)}{\alpha \sqrt{V_M^2 + V_N^2 + V_F^2}} \quad (12)$$

where α is a linearization approximation coefficient and is taken as 0.7 according to ASCE 7–16 [65]; V_M, V_F and V_N are the coefficients of variation for the material properties, fabrication procedure, and N, respectively; ϕ is a strength reduction factor; and N is the average ratio of $N_{ul,FE}$ to the corresponding design value [66]. According to the recommendations of AISC 360–16 [32], ϕ is taken as 0.75, and V_M and V_F are taken as 0.193 and 0.05, respectively, as suggested by Lai and Varma [66]. It is evident that determining the structure's safety level in a
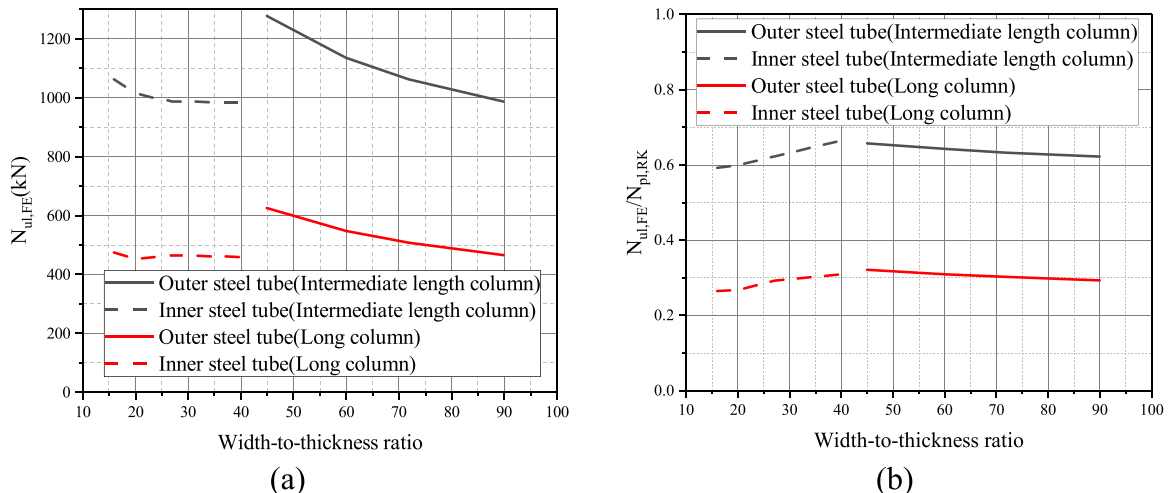

Fig. 25. Influence of different width-to thickness ratios on the ultimate strength of CFD-SSST slender columns.
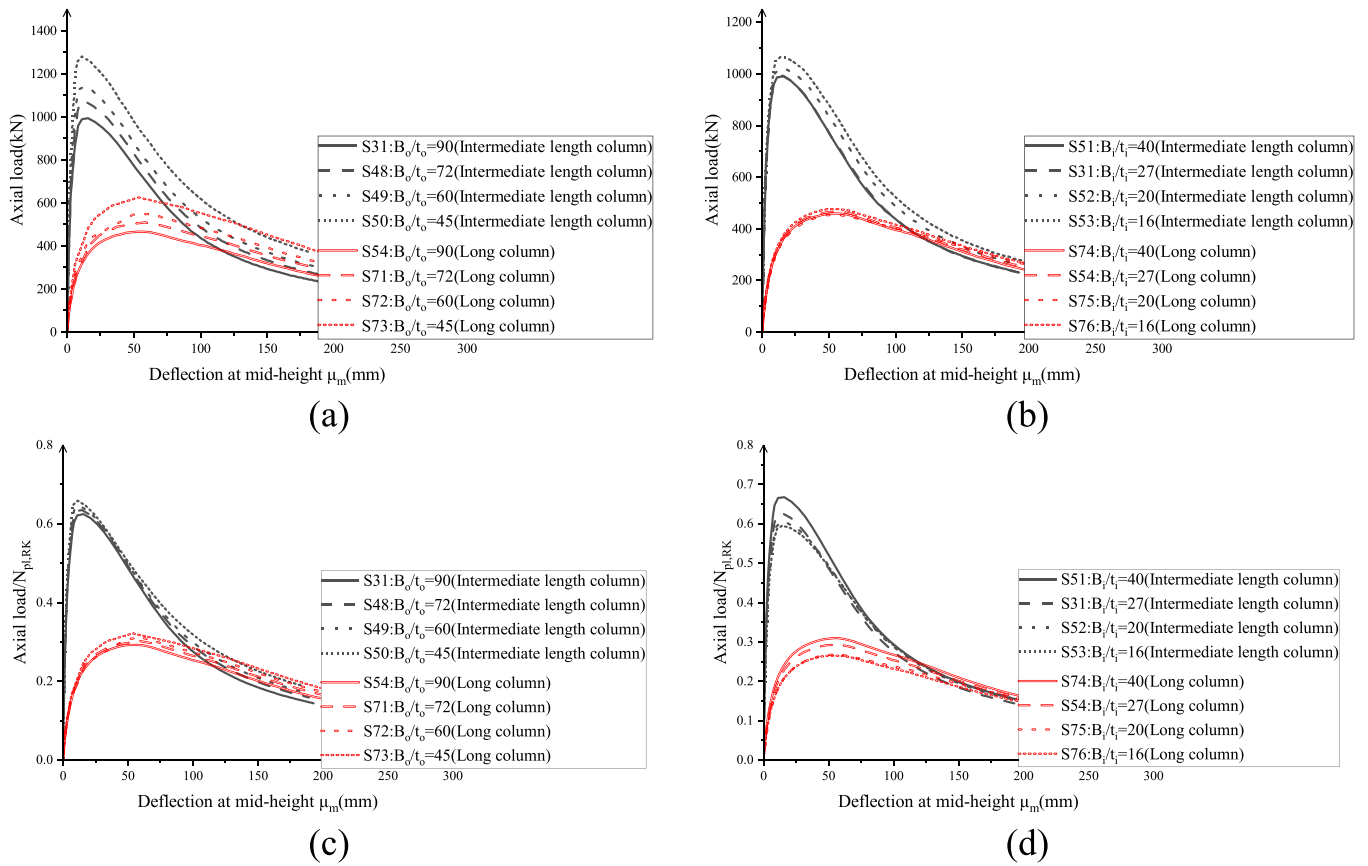
Fig. 26. Influence of different width-to thickness ratios on the (a) absolute strength- and (b) normalised strength-deflection relationships of CFD-SSST slender columns.
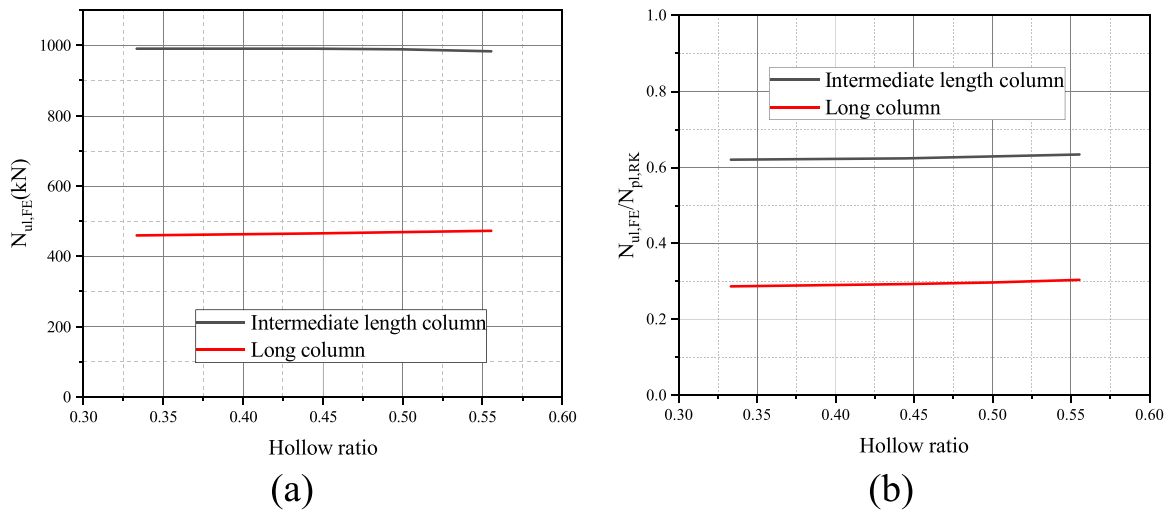

Fig. 27. Influence of hollow ratio on the ultimate strength of CFD-SSST slender columns.

practical and dependable way is challenging due to statistical factors resulting from changes in materials or loads. This is why the reliability analysis approach, which is founded on the theory of probability and statistics, takes into account uncertainties related to design variables for the safety design and evaluation of structures. To prevent abrupt failure or widespread damage progression, the target value for β in the case of overall buckling is 2.5 [32]. Therefore, if the reliability index (β) is greater than 2.5, even though some of the expected outcomes might be deemed unsafe, it guarantees the safety and integrity of any design method.

4.1. EN 1994 Part 1–1 [57]

The design process for CFD-SSST slender columns is expanded from Eurocode 4 Part 1–1 [57] (referred to as EC4-I in this context) for conventional CFST columns. According to EC4, the ultimate strength ($N_{ul,EC4}$) of a composite slender column can be ascertained using the slenderness reduction factor χ_{EC4} as follows:

$$N_{ul,EC4} = \chi_{EC4} \bullet N_{ul} \tag{13}$$

where χ is calculated using the instructions in EN 1993–1–1 [67] and shown in Eq. 14:

$$\chi_{EC4} = 1 \Big/ \left(\Phi + \sqrt{\Phi^2 - \bar{\lambda}^2} \right) \leq 1.0 \tag{14}$$

Φ is calculated as follows:

$$\Phi = 0.5 \bullet \left(1 + \alpha \bullet (\bar{\lambda} - 0.2) + \bar{\lambda}^2 \right) \tag{15}$$

It is noteworthy that the calculation of N_{cr}, as shown in Section 3, is based on N_{cr}, which in turn depends on the effective flexural stiffness, calculated as:

$$EI_{eff,EC4} = E_{so} \bullet I_{so} + E_{ss} \bullet I_{ss} + E_{si} \bullet I_{si} + 0.6 \bullet E_{cs} \bullet I_{cs} \tag{16}$$

According to Eq. 17, the section's ultimate strength ($N_{ul,EC4-I}$) is modified to encompass every element of the cross-section:

$$N_{ul,EC4-I} = A_{sy,eff} \bullet f_{yo} + A_{ss} \bullet f_{ys} + A_{si} \bullet f_{yi} + 0.85 \bullet A_{cs} \bullet f_{cs} \tag{17}$$

Notably, according to EN 1993–1–1 [67], the imperfection factor (α) is calculated as 0.49 based on buckling curve "c". Regarding CFST sections, EC4 [57] suggests that the coefficient of 0.85 be changed to 1.0. The EC4-II [57], another design resistance, is also computed without considering the decrease in concrete strength, as follows:

$$N_{ul,EC4-II} = A_{sy,eff} \bullet f_{yo} + A_{ss} \bullet f_{ys} + A_{si} \bullet f_{yi} + A_{cs} \bullet f_{cs} \tag{18}$$

4.2. AISC 360–16 [32]

The inner steel tube is incorporated into the design equations in AISC 360–16 [32] in a similar manner, thereby substituting the longitudinal and lateral reinforcing bars in the provided guidance for composite columns (CFSTs). Consequently, the CFD-SSST slender columns' ultimate strength ($N_{ul,AISC}$) is as follows:

$$N_{ul,AISC} = \begin{cases} N_{ul} \bullet \left[0.658^{\frac{N_{ul}}{N_e}} \right] & \dfrac{N_{ul}}{N_e} \leq 2.25 \\ \\ 0.877 \bullet N_e & \dfrac{N_{ul}}{N_e} \geq 2.25 \end{cases} \tag{19}$$

where N_e is the elastic critical buckling load calculated as $\left(\pi^2 (EI_{eff,AISC}) \right) / L_0^2$, and N_{ul} is the section's ultimate strength, as provided by Eq. 17. The effective flexural stiffness, or $EI_{eff,AISC}$, is calculated as follows:

$$EI_{eff,AISC} = E_{so} \bullet I_{so} + E_{ss} \bullet I_{ss} + E_{si} \bullet I_{si} + C_1 \bullet E_{cs} \bullet I_{cs} \tag{20}$$

where C_1 is a coefficient that is a function of the cross-sectional areas of the concrete and steel are denoted by Ac and As, respectively. It is determined using Eq. 21 to determine the effective rigidity of an encased composite compression member:

$$C_1 = 0.25 + 3 \bullet \left(\frac{A_s}{A_s + A_c} \right) \leq 0.7 \tag{21}$$

4.3. AS/NZS 2327 [34]

Design expressions for rectangular CFST columns are included in the AS/NZS 2327 [34] specification; these are modified for CFD-SSST slender columns in this instance. This code calculates the ultimate strength ($N_{ul,AS}$) of composite slender columns using a slenderness reduction factor χ_{AS}, which is modified as follows:

$$N_{ul,AS} = \chi_{AS} \left(A_{sy,eff} \bullet f_{yo} + A_{ss} \bullet f_{ys} + A_{si} \bullet f_{yi} + A_{cs} \bullet f_{cs} \right) \tag{22}$$

where:

$$\chi_{AS} = \xi \left[1 - \sqrt{1 - (90/\xi\lambda)^2} \right] \quad \text{with} \quad \xi = \frac{(\lambda/90)^2 + 1 + \eta}{2(\lambda/90)^2}, \quad \lambda = \lambda_\eta + \alpha_a \alpha_b,$$

$\eta = 0.00326(\lambda - 13.5) \geq 0$, $\quad \lambda_\eta = 90\lambda_r$, $\quad \alpha_a = \frac{2100(\lambda_\eta - 13.5)}{\lambda_\eta^2 - 15.3\lambda_\eta + 2050}$ $\quad$ and $\quad \alpha_b =$

$$\begin{cases} 0.5 \text{ if } k_f < 1 \\ 0 \text{ if } k_f = 1 \end{cases}, k_f = \frac{A_{sy,eff}}{A_{yo}}$$

Eq. 23 defines λ_r, which in these expressions refers to the relative slenderness of the composite column in a specified plane of bending:

$$\lambda_r = \sqrt{\frac{A_{sy,eff} f_{yo} + A_{ss} f_{ys} + A_{si} f_{yi} + A_{cs} f_{cs}}{\left(\frac{\pi^2 EI_e}{L_e^2} \right)}} \tag{23}$$

The effective elastic flexural stiffness, or EI_e, is calculated as follows:

$$EI_{e,AS} = E_{so} \bullet I_{so} + E_{ss} \bullet I_{ss} + E_{si} \bullet I_{si} + E_{cs} \bullet I_{cs} \tag{24}$$

4.4. ISO 16521–2024 [68]

The axial ultimate strength of trussed concrete-filled steel tubular (CFST) hybrid structures, as defined in ISO 16521–2024, has been adopted to estimate the ultimate load-bearing capacity ($N_{ul,ISO}$) of CFD-SSST slender columns. In accordance with this standard, the design axial strength is calculated by summing the resistances of the individual CFST chord cross-sections while accounting for global stability effects through the application of a stability reduction factor. This approach provides a simplified yet rational means of assessing the compressive performance of hybrid composite members incorporating dual stiffened steel tubes and infilled concrete.

$$N_{ul,ISO} = \chi_{ISO} \sum f_{sc} A_{sc} \tag{25}$$

where:

$$A_{sc} = A_{so} + A_{si} + A_{ss} + A_{cs} \quad , f_{sc} = \frac{f_{scy}}{\gamma_{msc}} \quad \text{and} \quad \gamma_{msc} \text{ is recommended}$$

as 1.2, according to GB/T 51446–2021[69], where f_{scy} is determined as:

$$f_{scy} = 1.18 + 0.85\xi_{ISO}\alpha_c f_{ck} \tag{26}$$

In this expression, $\xi_{ISO} = \frac{A_s f_y}{A_c \alpha_c f_{ck}}$, α_c is recommended as 0.83 for C40 concrete, $f_{ck} = 0.88\alpha_{c1}\alpha_{c2}f_{cu}$, and α_{c1} and α_{c2} are recommended as 0.76 and 1 for C40 concrete, respectively. χ_{ISO} is determined in accordance with Eq. (27):

$$\chi_{ISO} = \begin{cases} 1 & \text{if} \quad \lambda \leq \lambda_p \\ a\lambda^2 + b\lambda + c & \text{if} \quad \lambda_0 < \lambda \leq \lambda_p \\ d/(\lambda + 35)^2 & \text{if} \quad \lambda > \lambda_p \end{cases} \tag{27}$$

where:

$$a = \frac{1 + (35 + 2\lambda_p - \lambda_0)e}{(\lambda_p - \lambda_0)^2}$$

$$b = e - 2a\lambda_p,$$

$$c = 1 - a\lambda_0^2 - b\lambda_0,$$

$$d = \left[13500 + 4810\ln\left(\frac{235}{f_{oy}} \right) \right] \left(\frac{25}{\alpha_c f_{ck} + 5} \right)^{0.3} \left(\frac{\alpha_c}{0.1} \right)^{0.05}, \text{and}$$

$$e = \frac{-d}{(\lambda_p + 35)^3}$$

Moreover, λ_p and λ_0 are determined as : $\lambda_p = \dfrac{1811}{\sqrt{f_{oy}}}$ and λ_0

$$= \pi\sqrt{\frac{220\xi_{ISO} + 450}{(0.85\xi_{ISO} + 1.18)\alpha_c f_{ck}}},\ \text{respectively.}$$

4.5. Comparison of the design methods

The current section presents the results of a comparison between the values obtained using the various design methods and the ultimate axial loads predicted for different column arrangements by the FE model ($N_{ul,FE}$). The different design resistances against $N_{ul,FE}$ are shown in Fig. 28, and the numerical data, which includes the reliability index β, mean value, coefficient of variation (COV), and minimum and maximum values, is provided in Table 5.

As can be seen from Fig. 28 and Table 5, AS/NZS 2327 [34] offers the most accurate predictions, with most design values falling within 10 % of $N_{ul,FE}$. For $N_{ul,AS}/N_{ul,FE}$ ratios, the mean and COV (coefficient of variation) values are 0.99 and 0.101, respectively. Furthermore, this method's reliability index of 2.92 further supports its suitability as a design approach for the CFD-SSST thin columns. However, it should be noted that the other design methods [(Method-I) [57], (Method-II) [57], AISC [32], and ISO 16521–2024 [68]] predict mean design strength/FE strength ratios of 77 %, 83 %, 91 %, and 94 %, respectively, which generally underestimate the ultimate strength of CFDSST columns. Compared to the corresponding expressions in other design methods, the AS/NZS 2327 [34] approach does not reduce the concrete strength as is done in EC4 [57] (Method I). Furthermore, the effective flexural stiffness in AS/NZS 2327 is computed as the sum of the individual component flexural stiffnesses without applying a reduction to the concrete contribution. This results in a higher overall design strength, as the relative slenderness of the composite column is effectively reduced, thereby increasing the value of the buckling reduction factor, χ_{AS}, relative to alternative design approaches. To further examine this observation, a reduction factor for the concrete contribution to flexural stiffness (β_r) was derived based on the finite element modelling results. The relationship between β_r and the transverse slenderness parameter ($\bar{\lambda}$) is presented in Fig. 29. As shown, β_r remains close to unity across the studied range, which supports the validity of the $EI_{e,AS}$ formulation adopted by AS/NZS 2327 [34]. Additionally, Fig. 30 illustrates the relationship between the buckling reduction factor (χ) and the slenderness parameter for different design methods, revealing that EC4 [57] consistently yields the lowest χ values among the methods considered.
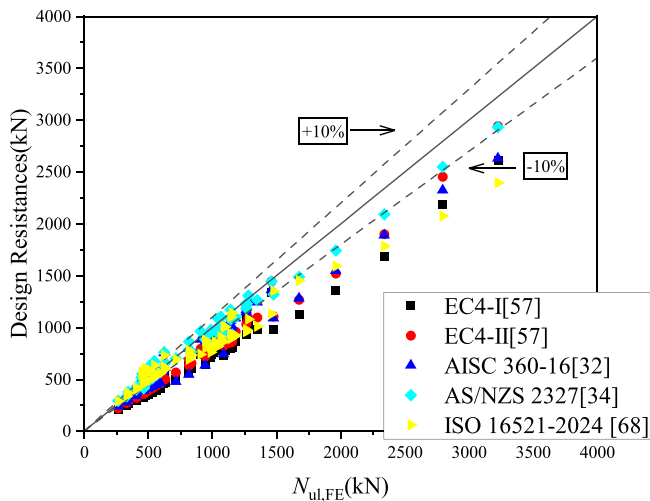
Table 5
Statistical evaluation of comparisons of different design strengths with the capacities obtained through FE modelling.

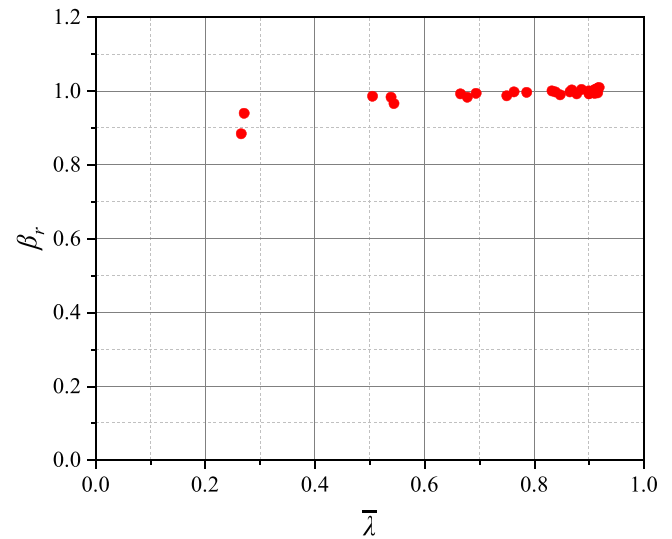| Statistics	EC4-I [57] $\dfrac{N_{ul,EC4-I}}{N_{ul,FE}}$	EC4-II [57] $\dfrac{N_{ul,EC4-II}}{N_{ul,FE}}$	AISC 360–16 [32] $\dfrac{N_{ul,AISC}}{N_{ul,FE}}$	AS/NZS 2327 [34] $\dfrac{N_{ul,AS}}{N_{ul,FE}}$	ISO 16521 [68] $\dfrac{N_{ul,ISO}}{N_{ul,FE}}$
Mean	0.77	0.83	0.91	0.99	0.94
COV	0.087	0.081	0.120	0.101	0.152
Max	0.92	0.99	1.21	1.24	1.28
Min	0.67	0.75	0.66	0.81	0.74
β	3.49	3.24	2.96	2.92	3.39

Fig. 29. Relationship between β_r *versus* $\bar{\lambda}$ based on FE results.
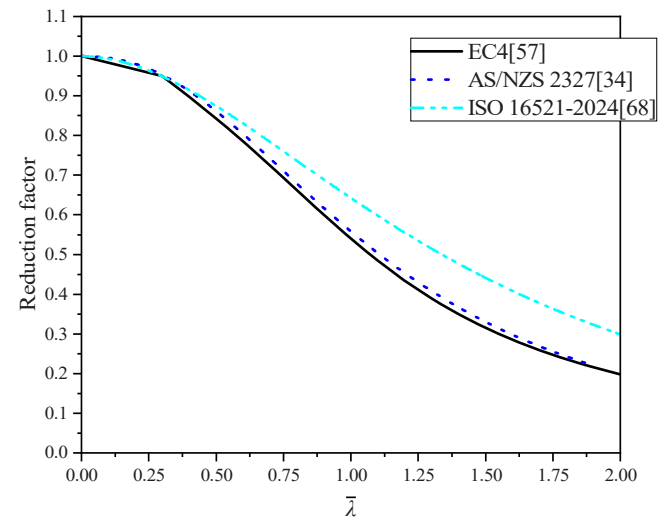

Fig. 30. Buckling reduction factor *versus* the slenderness parameter for different design methods.

5. Conclusions

The global buckling behaviour and ultimate strength of CFD-SSST slender columns—which have not been examined before—are investigated in this paper. The creation and validation of a finite element model are presented in the paper, with careful attention paid to ensuring that all necessary information is included that readers might find interesting.

Fig. 28. Comparison of different design strengths with the capacities obtained by the FE modelling.

A parametric study is then carried out using the validated model to determine the relative impact of different properties on the ultimate strength, failure mechanisms, and global buckling behaviour. The flexibility of existing design models is expanded to include the special characteristics of CFD-SSST slender columns, and their accuracy is evaluated. The following is a summary of the work's primary conclusions:

1. The axial strength and behaviour of CFD-SSST slender columns are significantly influenced by the slenderness ratio, as is well known for various composite columns. As anticipated, increasing the slenderness ratio of slender columns causes a change in the failure mode and a decrease in the load-carrying capacity.
2. A technique for dividing CFD-SSST slender columns into intermediate-length and long columns is presented, based on the results shown and the thorough examination of stress distributions and failure modes in particular.
3. The ultimate strength of CFD-SSST columns is higher than that of concrete-filled steel tubular (CFST) and concrete-fille dual tube (CFDSST) columns of the same weight because inner steel tubes enhance the cross-section's flexural stiffness and augment the load-carrying capacity.
4. The axial strength of intermediate-length CFD-SSST columns is clearly influenced by the yield strength of the outer steel tube, the sandwiched concrete strength, and the width-to-thickness ratio of the outer tube, according to parametric study results. In contrast, the axial strength of CFD-SSST long columns is marginally impacted by the sandwiched concrete strength and the width-to-thickness ratio of the outer tube.
5. The findings demonstrate that CFD-SSST slender columns with comparatively low hollow ratios work effectively and are probably going to offer the best outcome.
6. Various design processes from the available research literature and international design codes are evaluated, and it is demonstrated that AS/NZS 2327 [34] offers the most accurate predictions of those analysed.

A comprehensive cost-benefit analysis on the considered cross-section is still required (including material, construction, and maintenance costs). Moreover, the effects of unique properties of cold-formed steel and sandwiched concrete on reliability index calculation should be examined in future based on extensive testing.

CRediT authorship contribution statement

M.F. Hassanein: Conceptualization, Data curation, Formal analysis, Funding acquisition, Investigation, Methodology, Supervision, Visualization, Writing – original draft, Writing – review & editing. **Song-qi Jiang**: Writing – original draft, Validation, Resources, Methodology, Investigation, Formal analysis, Data curation, Conceptualization. **Yong-Bo Shao**: Writing – review & editing, Validation, Supervision, Resources, Investigation, Funding acquisition. **K.A. Cashell**: Writing – review & editing, Resources, Methodology, Investigation, Formal analysis.

Author statement

The authors' individual contributions have been outlined in Editorial Manager.

Declaration of Competing Interest

The authors declare that they have no known competing financial interests or personal relationships that could have appeared to influence the work reported in this paper.

Data availability

Data will be made available on request.

References

[1] Romero ML, Espinos A, Portolés JM, Hospitaler A, Ibañez C. "Slender double-tube ultra-high strength concrete-filled tubular columns under ambient temperature and fire". Eng Struct 2015;99:536–45.

[2] Albero V, Ibañez C, Piquer A, Hernández-Figueirido D. "Behaviour of slender concrete-filled dual steel tubular columns subjected to eccentric loads". J Constr Steel Res 2021;176(0):106365.

[3] Pons D, Espinós Ana, Albero V, Romero ML. "Numerical study on axial loaded ultra-high strength concrete-filled dual steel columns". Steel Compos Struct 2018; 26(6):705–17.

[4] Wan CY, Zha XX. "Nonlinear analysis and design of concrete-filled dual steel tubular columns under axial loading". Steel Compos Struct 2016;20(3):571–97.

[5] Chang X, Ru ZL, Zhou W, Zhang YB. "Study on concrete-filled stainless steel-carbon steel tubular (CFSCT) stub columns under compression". Thin-Walled Struct 2013; 63(0):125–33.

[6] Johansson M. "Composite Action and Confinement Effects in Tubular Steel-Concrete Columns". Ph.D. thesis. Goteborg, Sweden: Chalmers University of Technology; 2002.

[7] Han LH, Wei L, Bjorhovde R. "Developments and advanced applications of concrete-filled steel tubular (CFST) structures: members". J Constr Steel Res 2014; 100:211–28.

[8] Liu DL, Gho WM, Yuan J. "Ultimate capacity of high-strength rectangular concrete-filled steel hollow section stub columns". J Constr Steel Res 2003;59(12): 1499–515.

[9] Deng ZH, Guo JH, Yu JJ, Liu B. "Axial compression performance of coral concrete-filled aluminium tube (CCFAT) square stub columns". Case Stud Constr Mater 2021;15:e00697.

[10] Tao Z, Han LH, Wang ZB. "Experimental behaviour of stiffened concrete-filled thin-walled hollow steel structural (HSS) stub columns". J Constr Steel Res 2005;61(7): 962–83.

[11] Tao Z, Han LH, Wang DY. "Experimental behaviour of concrete-filled stiffened thin-walled steel tubular columns". Thin-Walled Struct 2007;45(5):517–27.

[12] Tao Z, Han LH, Wang D-Y. "Strength and ductility of stiffened thin-walled hollows steel structural stub columns filled with concrete". Thin-Walled Struct 2008;46 (10):1113–28.

[13] ACT-partner, advanced construction technology column, Accessed 21 August 2019, ⟨http://actpartner.co.kr⟩.

[14] Zhang YC, Chen Y. "Experimental study and finite element analysis of square stub columns with straight ribs of concrete-filled thin-walled steel tube". J Build Struct 2006;27(5):16–22.

[15] Dabaon MA, El-Boghbdadi MH, Hassanein MF. "Experimental investigation on concrete-filled stainless steel stiffened tubular stub columns". Eng Struct 2009;31 (2):300–7.

[16] Dabaon M, El-Khoriby S, El-Boghdadi M, Hassanein MF. "Confinement effect of stiffened and unstiffened concrete-filled stainless steel tubular stub columns". J Constr Steel Res 2009;65(8-9):1846–54.

[17] Wang ZB, Tao Z, Yu Q. "Axial compressive behaviour of concrete-filled double-tube stub columns with stiffeners". Thin-Walled Struct 2017;120:91–104.

[18] Zhang JH, Shao YB, Hassanein MF, Patel VI. "Axial compressive performance of ultra-high strength concrete-filled dual steel tubular columns with outer stiffened tubes and inner circular tubes". J Constr Steel Res 2023;203:107848.

[19] Wang ZB, Gao YH, Chi SY, Huang JZ. "Stability of composite concrete-filled square thin-walled steel tubular slender columns under axial compression". J Build Struct 2017;38(12):41–8 ([in Chinese]).

[20] Zhang JH, Shao YB, Hassanein MF, Cashell KA, Hadzima-Nyarko M. "Behaviour of ultra-high strength concrete-filled dual-stiffened steel tubular slender columns". Eng Struct 2024;300:117204.

[21] Wang ZB, Wei FB, Chi SY, Yu X. "Study on behaviour of composite concrete-filled square thin-walled steel tubular columns under eccentrical compression". J Hunan Univ (Nat Sci) 2018;45(9):43728.

[22] Wang ZB, Zhang WA, Chi SY, Li YJ. "Flexural behaviour of composite concrete-filled square thin-walled steel tubular specimens". J Build Struct 2017;38(7):78–84 ([in Chinese]).

[23] Wang ZB, Guo JT, Zhang WA, Zheng YQ. "Hysteretic behaviour of concrete-filled square cold-formed thin-walled steel tubular beam-columns". J Build Struct 2019; 40(11):172–81 ([in Chinese]).

[24] Wang ZB, Wu HJ, Zhuang JP, Yu X, Zhang WA. "Seismic behaviour of concrete-filled thin-walled double-tubular columns with longitudinal stiffeners". J Build Struct, Vo 2020;41(11):41–50 ([in Chinese]).

[25] Zhang JH, Shao YB, Hassanein MF, Cashell KA, Hadzima-Nyarko M. "Behaviour of cold-formed concrete-filled dual steel stiffened tubular short columns". J Constr Steel Res 2024;213:108381.

[26] Neogi P, Sen H, Chapman J. "Concrete-filled tubular steel columns under eccentric loading", The Structural. Engineer 1969;47:187–95.

[27] Knowles R, Park R. Strength of concrete-filled steel tubular column, Journal of the Structural Division. ASCE 1969;95:2565–87.

[28] Schurgacz P, Winkler R, Knobloch M. Experimental investigation on innovative stub and slender composite columns with high-performance materials. J Constr Steel Res 2025;230:109544.

[29] Zhao H, Wang R, Lam D, Hou CC, Zhang R. Behaviours of circular CFDST with stainless steel external tube: Slender columns and beams. Thin-Walled Struct 2021; 158:107172.

[30] Han LH, Lam D, Nethercot D. Design guide for concrete-filled double skin steel tubular structures. CRC Press; 2018.

[31] GB 50936-2014, Technical code for concrete filled steel tubular structures, Chinese Standard, China, 2014.

[32] AISC 360-16, Specification for structural steel buildings, American Institute of Steel Construction, Chicago, 2016.

[33] Hassanein MF, Shao YB, Zhang JH, Cashell KA, Elsisy AR. Global buckling behaviour and design of square cold-formed concrete-filled dual steel stiffened slender columns. J Constr Steel Res 2024;218:108706.

[34] AS/NZS 2327, Composite structures-Composite steel-concrete construction in buildings, Australian/New Zealand Standard, Australian, 2017.

[35] Luan, W.L., (2019), "Study on the mechanical behavior of concrete filled stiffened square steel tubular middle long column under axial compression", Master, Inner Mongolia University of Science & Technology, Bao Tou. [in Chinese].

[36] Wang WD, Ji SH, Shi YL. "Experimental and numerical investigations on concrete-filled double-tubular slender columns under axial and eccentric loading". J Constr Steel Res 2023;201:107714.

[37] ABAQUS, ABAQUS Standard User's Manual, Version 2020, Dassault Systèmes Corp, Providence (RI, USA), 2020.

[38] Gardner L, Yun X. "Description of stress-strain curves for cold-formed steels,". Constr Build Mater 2018;189:527–38.

[39] Abdelrahman AHA, Liu S, Liu YP, Chan SL. Simulation of Thin-Walled Members with Arbitrary-Shaped Cross-Sections for Static and Dynamic Analyses. Int J Struct Stab Dyn 2020;20(12):2050128.

[40] Tao Z, Wang ZB, Yu Q. "Finite element modelling of concrete-filled steel stub columns under axial compression". J Constr Steel Res 2013;89:121–31.

[41] Mander JB, Priestley MJN, Park R. Theoretical. Stress-strain Model Confin Concr, J Struct Eng 1988;114(8):1804–26.

[42] Sakino K, Nakahara H, Morino S, et al. Behavior of centrally loaded concrete-filled steel tube short columns. J Struct Eng 2004;130(2):180–8.

[43] Zhou Z, Gan D, Zhou X. Improved composite effect of square concrete-filled steel tubes with diagonal binding ribs. J Struct Eng 2019;145(10):1–12. pp. 04019112.

[44] Huang WF, Shao YB, Hassanein MF, et al. Experimental and numerical investigation of square concrete-filled double-skin steel stiffened tubular stub columns with CHS inner tubes under axial compression. Thin-Walled Struct 2024; 199:111792.

[45] Zhang JH, Hassanein MF, Cashell KA. Experimental and numerical investigation on the behaviour of square concrete-filled cold-formed double-skin steel stiffened tubular short columns, Engineering. Structure 2024;303:117560.

[46] Gardner L, Nethercot DA. "Numerical modelling of stainless steel structural components-A consistent approach". J Struct Eng 2004;130(10):1586–601.

[47] Ellobodya E, Young B. "Structural performance of cold-formed high strength stainless steel columns". J Constr Steel Res 2005;61(12):1631–49.

[48] Tao Z, Uy B, Han LH, et al. "Analysis and design of concrete-filled stiffened thin-walled steel tubular columns under axial compression". Thin-Walled Struct 2009; 47(12):1544–56.

[49] GB50018-2002, Technical code of cold-formed thin-wall steel structures, Chinese Standard, China, 2002.

[50] Li GW, Li YQ, Xu J, Cao X. Experimental investigation on the longitudinal residual stress of cold-formed thick-walled SHS and RHS steel tubes. Thin-Walled Struct 2025;138:473–84.

[51] Zhou Z, Gan D, Zhou X. Improved composite effect of square concrete-filled steel tubes with diagonal binding ribs. J Struct Eng 2019;145(10):1–12. pp. 04019112.

[52] GB 50017-2017, Standard for design of steel structures, China Building Industry Press, Beijing, 2017.

[53] Zhang L, Mao CX, Li XG. Experimental study on CFNRST members under combined compression and bending. J Constr Steel Res 2020;167:105950.

[54] Huang Y, Lu Y, Ma W. Experimental and numerical investigation on axial behavior of circular and square slender reinforced columns. J Constr Steel Res 2024;213: 108417.

[55] Hassanein MF, Elchalakani M, Pater VI. "Overall buckling behaviour of circular concrete-filled dual steel tubular columns with stainless steel external tubes". Thin-Walled Struct 2017;115:336–48.

[56] DBJ/T13-51-2010, Technical specification for concrete filled steel tubular structures, The Construction Department of Fujian Province, Fuzhou, China, 2010 (in Chinese).

[57] Eurocode 4, Design of composite steel and concrete structures, Part 1.1, General rules and rules for building, British Standards Institution, London, (BS EN 1994-1-1: 2004).

[58] AISC-LRFD-99, Load and Resistance Factor Design Specification for Structural Steel Buildings, American Institute of Steel Construction, Chicago, 1999.

[59] Tao Z, Han L-H, Zhao XL. Behaviour of concrete-filled double skin (CHS Inner and CHS Outer) steel tubular stub columns and beam-columns. J Constr Steel Res 2004; 60(8):1129–58.

[60] Yang Y-F, Fu F, Bie X-M, Dai X-H. "Axial compressive behaviour of CFDST stub columns with large void ratio". J Constr Steel Res 2021;186:106892.

[61] Shi Y-L, Ji S-H, Wang W-D, Xian W, Fan J-H. "Axial compressive behaviour of tapered CFDST stub columns with large void ratio". J Constr Steel Res 2022;191: 107206.

[62] Eurocode 3, Design of steel structures, Part 4.4, Plate elements without longitudinal stiffeners, British Standards Institution, London, 1997 (BS EN 1993-1-5: 1997).

[63] Ayough P, Ibrahim Z, Ramli Sulong NH, Hsiao P-C, Elchalakani M. "Numerical analysis of square concrete-filled double skin steel tubular columns with rubberized concrete". Structures 2021;32:1026–47.

[64] Thai S, Thai H-T, Uy B, Ngo T. "Concrete-filled steel tubular columns: test database, design and calibration". J Constr Steel Res 2019;157:161–81.

[65] ASCE. (2017), "Minimum design loads for buildings and other structures", ASCE 7-10, Reston, VA.

[66] Lai Z, Amit HVarma. "High-Strength rectangular CFT Memb: Database, Model, Des Short Columns", J Struct Eng 2018;144(5):04018036.

[67] Eurocode 3, Design of steel structures, Part 1.1, General rules and rules for buildings, British Standards Institution, London, 2004 (BS EN 1993-1-1: 2004).

[68] ISO 16521-2024, Design of concrete-filled steel tubular (CFST) hybrid structures, International Organization for Standardization, 2024.

[69] GB/T 51446-2021, Technical standard for concrete-filled steel tubular hybrid structures, Chinese Standard, China, 2021.